Biogeosciences Discuss., 11, 13067–13126, 2014
www.biogeosciences-discuss.net/11/13067/2014/
doi:10.5194/bgd-11-13067-2014

Biogeosciences Discussions
Open Access

Organic carbon production, mineralization and preservation on the Peruvian margin

A. W. Dale[1], S. Sommer[1], U. Lomnitz[1], I. Montes[2], T. Treude[1], J. Gier[1], C. Hensen[1], M. Dengler[1], K. Stolpovsky[1], L. D. Bryant[1], and K. Wallmann[1]

[1]GEOMAR Helmholtz Centre for Ocean Research Kiel, Kiel, Germany
[2]Instituto Geofísico del Perú (IGP), Lima, Perú

Received: 15 August 2014 – Accepted: 16 August 2014 – Published: 9 September 2014

Correspondence to: A. W. Dale (adale@geomar.de)

Published by Copernicus Publications on behalf of the European Geosciences Union.

Abstract

Carbon cycling in Peruvian margin sediments (11° S and 12° S) was examined at 16 stations from 74 m on the inner shelf down to 1024 m water depth by means of in situ flux measurements, sedimentary geochemistry and modeling. Bottom water oxygen was below detection limit down to ca. 400 m and increased to 53 µM at the deepest station. Sediment accumulation rates and benthic dissolved inorganic carbon fluxes decreased rapidly with water depth. Particulate organic carbon (POC) content was lowest on the inner shelf and at the deep oxygenated stations (< 5 %) and highest between 200 and 400 m in the oxygen minimum zone (OMZ, 15–20 %). The organic carbon burial efficiency (CBE) was unexpectedly low on the inner shelf (< 20 %) when compared to a global database, for reasons which may be linked to the frequent ventilation of the shelf by oceanographic anomalies. CBE at the deeper oxygenated sites was much higher than expected (max. 81 %). Elsewhere, CBEs were mostly above the range expected for sediments underlying normal oxic bottom waters, with an average of 51 and 58 % for the 11° S and 12° S transects, respectively. Organic carbon rain rates calculated from the benthic fluxes alluded to a very efficient mineralization of organic matter in the water column, with a Martin curve exponent typical of normal oxic waters (0.88 ± 0.09). Yet, mean POC burial rates were 2–5 times higher than the global average for continental margins. The observations at the Peruvian margin suggest that a lack of oxygen does not affect the degradation of organic matter in the water column but promotes the preservation of organic matter in marine sediments.

1 Introduction

The Peruvian upwelling forms part of the boundary current system of the Eastern Tropical South Pacific and is one of the most biologically productive regions in the world (Pennington et al., 2006). Respiration of organic matter in subsurface waters leads to the development of an extensive and perennial oxygen minimum zone, OMZ (Walsh,

BGD
11, 13067–13126, 2014

1981; Quiñones et al., 2010). Bottom water dissolved oxygen (O_2) concentrations have been measured to be below the analytical detection limit from the shelf down to ca. 400 m (Gutiérrez et al., 2008; Bohlen et al., 2011). Sediments within this depth interval display organic carbon contents in excess of 15 % (Reimers and Suess, 1983a; Suess et al., 1987; Arthur and Dean, 1998); much higher than the average continental margin of ca. 0.5–2 % (Seiter et al., 2004).

Oxygen deficient regions like Peru have been described as modern analogues for ancient ocean anoxic events; periods of widespread oxygen depletion in the geological past (Demaison and Moore, 1980). During those periods, massive amounts of organic carbon were buried to the long-term sedimentary record (Schlanger and Jenkyns, 1976). Burial of organic carbon represents a net removal of carbon dioxide from the atmosphere and a source of atmospheric oxygen (Berner, 1982). An understanding of the factors that drive enhanced carbon preservation and burial in marine sediments is, therefore, of utmost importance for improving the predictive capabilities of global carbon cycle models on geological time scales (Berner, 2004; Wallmann and Aloisi, 2012).

Pioneering workers argued that carbon preservation and burial is mainly driven by the absence of O_2 in the bottom water (Demaison and Moore, 1980) or the increased carbon rain rate to the seafloor due to higher primary productivity (Pedersen and Calvert, 1990). Since then, much work on the biogeochemical characteristics of sediments has been undertaken to better disentangle these factors (Hedges and Keil, 1995; Arthur and Dean, 1998; Keil and Cowie, 1999; Vanderwiele et al., 2009; Zonneveld et al., 2010; Moodley et al., 2011 and many others). These studies do seem to indicate that sediments under anoxic or oxygen-deficient waters are, broadly speaking, geochemically different from those under normal oxic bottom waters. Much less certain, however, is the question of whether the bulk preservation of organic carbon in sediments is indeed favored by the absence of O_2 (Reimers and Suess, 1983a; Westrich and Berner, 1984; Calvert et al., 1992; Canfield, 1993; Hedges and Keil, 1995; Hulthe et al., 1998; Burdige, 2007). Investigations in the water column have shown that respi-

BGD
11, 13067–13126, 2014

ration of organic carbon is significantly reduced in oxygen-deficient waters, leading to elevated carbon fluxes to the sediments (Martin et al., 1987; Devol and Hartnett, 2001; Van Mooy et al., 2002).

Quantification of the organic carbon burial efficiency in sediments (CBE) requires at least two of the following three pieces of information, (i) the rain rate of organic carbon to the sediment, (ii) the rate of carbon burial at the sediment depth where degradation no longer occurs significantly, and (iii) the depth-integrated rate of organic carbon oxidation (Burdige, 2007). That is, at steady-state, (i) = (ii) + (iii). They are typically quantified using (in the same order) (i) sediment trap particle fluxes, (ii) sedimentation rates (using radioactive isotopes) combined with carbon content measurements, and (iii) stoichiometric mass balances or benthic fluxes. Each of these approaches integrates the carbon flux over time-scales that differ enormously, for example, from days to weeks for traps to hundreds or thousands of years for burial (Burdige, 2007). Data from sediment traps are associated with additional uncertainties, perhaps the most important being that they do not adequately capture particulate resuspension and transport in the benthic boundary layer. Still, with these caveats in mind, bulk measurements of the influx/outflux of carbon to/from the surface sediment layer are currently the most reliable means of calculating the CBE.

Rates of carbon burial and mineralization on the Peruvian margin have been studied as part of the Collaborative Research Center 754 (Sonderforschungsbereich, SFB 754, www.sfb754.de/en) "Climate–Biogeochemistry Interactions in the Tropical Ocean" (first phase 2008–2011 and second phase 2012–2015). The overall aim of the SFB 754 is to understand the physical and biogeochemical processes that lead to the development and existence of oxygen-deficient regions in the tropical oceans. In this paper, in situ benthic fluxes and sedimentary geochemical data collected during two campaigns to the Peruvian margin at 11° S and 12° S during the SFB 754 are used to summarize our current understanding of carbon cycling in this setting. We address the following questions:

BGD
11, 13067–13126, 2014

1. What is the rate of organic carbon mineralization and burial in the sediments down through the OMZ? Do these data point toward diminished rates of organic carbon mineralization in the water column?

2. Which factors determine the CBE at Peru and is there any marked difference for stations underlying oxic and anoxic bottom waters?

Companion papers address alternative aspects of the functioning of OMZs, including the ventilation physics and regional oxygen variability in the Eastern Tropical North Atlantic (Brandt et al., 2014), pelagic biogeochemistry (Löscher et al., unpub. data), paleoceanography (Schönfeld et al., 2014) and physical and biogeochemical dynamics inferred from numerical modeling (Oschlies et al., unpub. data).

2 Study area

Equatorward winds engender upwelling of nutrient-rich Equatorial subsurface water along the Peruvian coast (Fiedler and Talley, 2006). Upwelling is most intense between 5 and 15° S where the shelf narrows (Quiñones et al., 2010). Highest rates of primary productivity (1.8–3.6 g C m^{-2} d^{-1}) are 6 months out of phase with upwelling intensity presumably due to the variability in the mixed layer depth that deepens during the windy upwelling period (Walsh, 1981; Echevin et al., 2008; Quiñones et al., 2010). Austral winter and spring is the main upwelling period with interannual variability imposed by the El Niño Southern Oscillation (ENSO) (Morales et al., 1999). Neutral or negative ENSO conditions prevailed at the time of sampling (November 2008 for 11° S and January 2013 for 12° S) (http://www.cpc.ncep.noaa.gov). The lower vertical limit of the OMZ is around 700 m water depth off Peru (OMZ defined by dissolved oxygen (O_2) < 20 µmol kg^{-1}; Fuenzalida et al., 2009). The mean depth of the upper boundary of the OMZ on the shelf at 11° S and 12° S is around 50 m (Gutiérrez et al., 2008), but deepens to ca. 200 m or more during ENSO years (e.g. Levin et al., 2002). At these times, dissolved O_2 on the shelf can vary between 0 and 100 µM within a matter of

BGD
11, 13067–13126, 2014

days to weeks as opposed to several months during weaker ENSO events (Gutiérrez et al., 2008; Scholz et al., 2011; Noffke et al., 2012).

Sediments at 11 and 12° S are carbonate poor, diatomaceous muds with high accumulation rates (Suess et al., 1987, and many others). Surface particulate organic carbon (POC) content is high in the core of the OMZ (15 to 20 %) with lower values (5 to 10 %) on the shelf and in deep waters (Böning et al., 2004). $\delta^{13}C$ analysis and other geochemical indicators confirm that the organic matter at this latitude is almost entirely of marine origin (Arthur and Dean, 1998; Reimers and Suess, 1983b; Levin et al., 2002; Gutiérrez et al., 2009). There are no major rivers supplying significant amounts of terrestrial organic material. The surface sediments are gelatinous and cohesive down to roughly 400 m, ranging from dark olive green to black in color with no surface-oxidized layer (Bohlen et al., 2011; Mosch et al., 2012). The surface is colonized by dense, centimeter-thick mats of gelatinous sheaths containing microbial filaments of the large sulfur oxidizing bacteria *Thioploca* spp. (Henrichs and Farrington, 1984; Arntz et al., 1991). These bacteria are able to glide through the sediments to access sulfide which they oxidize using nitrate stored within intracellular vacuoles (Jørgensen and Gallardo, 2006). The bacterial density varies with time on the shelf depending on the bottom water redox conditions (Gutiérrez et al., 2008). Below the OMZ, the sediments are olive green throughout with a thin upper oxidized layer light green/yellow in color (Bohlen et al., 2011; Mosch et al., 2012). Spionid polychaetes (ca. 2 cm length) have been observed in association with the mats; other larger epibenthic megafauna are restricted to oxygen-containing waters below the OMZ (Mosch et al., 2012).

For the purposes of this study, we divide the Peruvian margin into 3 zones broadly reflecting bottom water O_2 distributions and sedimentary POC content: (i) the inner and outer shelf (< ca. 200 m, POC 5 to 10 %, O_2 < d.l. at time of sampling) where non-steady conditions are occasionally driven by periodic intrusion of oxygenated bottom waters (Gutiérrez et al., 2008), (ii) the OMZ (ca. 200 to 450 m, POC 10–20 %, O_2 < d.l. at time of sampling) where O_2 is predominately below detection limit, and (iii) the deep

BGD
11, 13067–13126, 2014

stations below the OMZ with oxygen-containing bottom water (POC ≤ ca. 5 % and O_2 > d.l.).

3 Material and methods

3.1 Flux measurements and sediment sampling

We present data from 6 stations along 11° S sampled during expedition M77 (cruise legs 1 and 2) in November 2008 and 10 stations along 12° S during expedition M92 (leg 3) in January/February 2013, both on RV *Meteor*. Sampling stations are shown in Fig. 1. Both campaigns took place during austral summer, i.e. the low upwelling season. With the exception of the particulate phases, the geochemical data and benthic modeling results from the 11° S transect have been published previously (Bohlen et al., 2011; Scholz et al., 2011; Mosch et al., 2012; Noffke et al., 2012). Data from 12° S are new to this study.

In situ fluxes were measured using data collected from Biogeochemical Observatories, BIGO (Sommer et al., 2008; Sommer et al., unpub. data). BIGO landers contained two circular flux chambers (internal diameter 28.8 cm, area 651.4 cm^2). One lander at 11° S, BIGO-T, contained only one benthic chamber. Each chamber was fitted with an optode to monitor dissolved O_2 concentrations. A TV-guided launching system allowed smooth placement of the observatories at selected sites on the sea floor. Two hours after the landers were placed on the sea floor, the chamber(s) were slowly driven into the sediment (~ 30 cm h^{-1}). During this initial period, the water inside the flux chamber was periodically replaced with ambient bottom water. After the chamber was fully driven into the sediment, the chamber water was again replaced with ambient bottom water to flush out solutes that might have been released from the sediment during chamber insertion. The water volume enclosed by the benthic chamber ranged from 8.5 to 18.5 L. During the BIGO-T experiments, the chamber water was replaced with ambient bottom

BGD
11, 13067–13126, 2014

water half way through the deployment period to restore outside conditions and then re-incubated.

Four (11° S) or eight (12° S) sequential water samples were removed periodically with glass syringes (volume of each syringe ~ 47 mL) to determine fluxes of solutes across the sediment–water interface. For BIGO-T, 4 water samples were taken before and after replacement of the chamber water. The syringes were connected to the chamber using 1 m long Vygon tubes with an internal volume of 6.9 mL. Prior to deployment, these tubes were filled with distilled water, and great care was taken to avoid enclosure of air bubbles. Concentrations were corrected for dilution using measured chloride concentrations in the syringe and bottom water. Water samples for measurements of pCO_2 (12° S) were taken at four regular time intervals using 80 cm long glass tubes (internal volume ca. 15 cm^3). An additional syringe water sampler (four or eight sequential samples) was used to monitor the ambient bottom water. The sampling ports for ambient seawater were positioned 30–40 cm above the seafloor. The incubations were conducted for time periods ranging from 17.8 to 33 h. Immediately after retrieval of the observatories, the water samples were transferred to the onboard cool room (8 °C) for further processing and sub-sampling.

Sediment samples for analysis were taken using both MUC and BIGO technologies. In this paper we report on MUC data only since the core length (ca. 20–40 cm) was typically much greater than the short BIGO cores (ca. 10 cm). Furthermore, MUC data are unaffected by possible artifacts arising from insertion of the roller underneath the chambers at the end of the BIGO deployments. Retrieved cores were immediately transferred to a cool room onboard at 4 °C and processed within a few hours. Subsampling for redox sensitive constituents was performed under anoxic conditions using an argon-filled glove bag. Sediment samples for porosity analysis were transported to the onshore laboratory in air-tight containers at 4 °C. Sediment sections for porewater extraction were transferred into tubes pre-flushed with argon gas and subsequently centrifuged at 4500 rpm for 20 min. Prior to analysis, the supernatant porewater was filtered with 0.2 µm cellulose acetate Nuclepore® filters inside the glove bag. The cen-

BGD
11, 13067–13126, 2014

trifugation tubes with the remaining solid phase of the sediment were stored at −20 °C for further analysis onshore. Additional samples for bottom water analysis were taken from the water overlying the sediment cores.

3.2 Analytical details

Dissolved oxygen concentrations in the water column were measured using a Seabird SBE43 sensor mounted on a SeaBird 911 CTD rosette system. The optodes were calibrated by vigorously bubbling filtered seawater from the bottom water at each station with air and with argon for 20 min. The sensors were calibrated against discrete samples collected from the water column on each CTD cast and analyzed onboard using Winkler titration with an onboard detection limit of ca. 5 µM. However, O_2 concentrations at sub-micromolar levels were measured within the core of the OMZ using microsensors (Kalvelage et al., 2013). For the purposes of this study, therefore, we broadly define O_2 concentrations below the detection limit of the Winkler analysis as anoxic.

Ammonium (NH_4^+), nitrite (NO_2^-), dissolved ferrous iron (Fe^{2+}), phosphate (PO_4^{3-}) and dissolved sulfide (H_2S) were measured onboard using standard photometric techniques with a Hitachi U2800 photometer (Grasshoff et al., 1999). Aliquots of porewater were diluted with O_2-free artificial seawater prior to analysis where necessary. Porewater samples for Fe^{2+} analysis were treated with ascorbic acid directly after filtering (0.2 µm) inside the glove bag. Detection limits for NO_3^-, NH_4^+ and TH_2S were 1 µM, 5 µM for PO_4^{3-} and 0.1 µM for NO_2^-. Total alkalinity (TA) was determined onboard by direct titration of 1 mL porewater with 0.02 M HCl using a mixture of methyl red and methylene blue as indicator and bubbling the titration vessel with Ar gas to strip CO_2 and H_2S. The analysis was calibrated using IAPSO seawater standard, with a precision and detection limit of 0.05 meq L^{-1}. Ion chromatography (Methrom 761) was used to determine sulfate (SO_4^{2-}) in the onshore laboratory with a detection limit of < 100 µM and precision of 200 µM. Major cations were determined by ICP-AES with precision

BGD
11, 13067–13126, 2014

and relative accuracy as given by Haffert et al. (2013). Analytical details of dinitrogen gas (N_2) measurements, used a model constraint on benthic N turnover, are described by Sommer et al. (unpub. data).

Partial pressure of CO_2 (pCO_2) was analyzed in the benthic chambers at 12° S. pCO_2 analysis was performed onboard by passing the sample from the glass tubes (without air contact) through the membrane inlet of a mass spectrometer (GAM200 IPI Instruments, Bremen). The samples were analyzed sequentially by switching from one tube to another and flushed with distilled water between samples. Standards were prepared by sparging filtered seawater from the bottom water from each station using standard bottles of CO_2 of known concentration at in situ temperature for 30 min. The relative precision of the measurement was < 1 %.

Wet sediment samples for analysis of POC, PON and total particulate sulfur (TPS) were freeze-dried in the onshore laboratory and analyzed using a Carlo-Erba element analyzer (NA 1500). POC content was determined on the residue after acidifying the sample with HCl to release the inorganic components as CO_2. Inorganic carbon was determined by weight difference. The precision and detection limit of the analysis was 0.04 and 0.05 dry weight percent (%), respectively. Porosity was determined in the onshore laboratory from the weight difference of the wet and freeze-dried sediment. Values were converted to porosity (water volume fraction of total sediment) assuming a dry sediment density of 2 g cm^{-3} (Böning et al., 2004) and seawater density of 1.023 g cm^{-3}.

Additional samples from adjacent MUC liners taken from the same cast were used for the determination of down-core profiles of unsupported $^{210}Pb_{xs}$ (excess) activity. Between 5 and 34 g of freeze-dried and ground sediment, each averaging discrete 2 cm depth intervals, was embedded into a 2-phase epoxy resin (West System Inc.). Following Mosch et al. (2012), a low-background coaxial Ge(Li) planar detector (LARI, University of Göttingen) was used to measure total ^{210}Pb via its gamma peak at 46.5 keV and ^{226}Ra via the granddaughter ^{214}Pb at 352 keV. Prior to analysis, the gas-tight embedded sediment was allowed to equilibrate between ^{226}Ra and ^{214}Pb for at least three

BGD
11, 13067–13126, 2014

weeks. In order to determine the unsupported fraction ($^{210}Pb_{xs}$), the measured total ^{210}Pb activity of each sample was corrected by subtracting its individual ^{226}Ra activity, assuming post-burial closed system behavior. The relative error of the measurements (2σ) ranged between 8 and 58 %. Uncertainty of the calculated $^{210}Pb_{xs}$ data derives from the individual measurement of ^{210}Pb and ^{226}Ra activities according to standard propagation rules. The down-core decrease in $^{210}Pb_{xs}$ and sediment porosity allows the determination of sediment accumulation and bioturbation rates (see below). For some cores, the radiometric lead chronology was validated with the detection of the anthropogenic enrichment peak of nuclide ^{241}Am (co-analysed on 60 keV) as an independent time marker in the profiles, originating from nuclear tests in the Southern Hemisphere during the early 1960s (data not shown).

3.3 Calculation of dissolved inorganic carbon (DIC) fluxes

DIC concentrations in the benthic chambers at 12° S were calculated from the concentrations of TA and pCO_2 using the equations and equilibrium coefficients given by Zeebe and Wolf-Gladrow (2001). pCO_2 and TA concentrations increased linearly with time inside the chambers and there were no spurious outliers such that all measurements were used. Since four samples for pCO_2 were taken using the glass tubes vs. eight samples for TA analysis in the syringes, each successive pair of TA data were averaged for calculating DIC. A constant salinity of 35 (psu), total boron concentration of 0.418 mM and seawater density of 1.025 kg L^{-1} were assumed. Corrections were made for the occurrence of free hydrogen sulfide in the bottom water at the shelf stations. DIC fluxes were calculated from the concentrations as described above.

3.4 Determination of sediment accumulation rates

Particle-bound $^{210}Pb_{xs}$ is subject to mixing in the upper sediment layers by the movement of benthic fauna. The distribution of $^{210}Pb_{xs}$ can thus be used to determine bioturbation coefficients as well as sedimentation rates using modeling approaches. We

BGD
11, 13067–13126, 2014

simulated the activity of $^{210}Pb_{xs}$ in Bq g^{-1} using a steady state numerical model that includes terms for sediment burial, mixing (bioturbation), compaction and radioactive decay:

$$(1-\varphi(x))\cdot\rho\cdot\frac{\partial^{210}Pb_{xs}(x)}{\partial t}=\frac{\partial\left((1-\varphi(x))\cdot\rho\cdot D_B(x)\cdot\frac{\partial^{210}Pb_{xs}(x)}{\partial x}\right)}{\partial x} - \frac{\partial\left((1-\varphi(x))\cdot\rho\cdot v_s(x)\cdot^{210}Pb_{xs}(x)\right)}{\partial x}+(1-\varphi(x))\cdot\rho\cdot\lambda\cdot^{210}Pb_{xs}(x) \quad (1)$$

In this equation, t (yr) is time, x (cm) is depth below the sediment–water interface, $\varphi(x)$ (dimensionless) is porosity, $v_s(x)$ (cm yr^{-1}) is the burial velocity for solids, $D_B(x)$ (cm^2 yr^{-1}) is the bioturbation coefficient, λ (0.03114 yr^{-1}) is the decay constant for $^{210}Pb_{xs}$ and ρ is the bulk density of solid particles (2.0 g cm^{-3}, Böning et al., 2004).

Porosity was described using an exponential function assuming steady-state compaction:

$$\varphi(x)=\varphi(L)+(\varphi(0)-\varphi(L))\cdot\exp\left(-\frac{x}{z_{por}}\right) \quad (2)$$

where $\varphi(0)$ is the porosity at the sediment–water interface, $\varphi(L)$ is the porosity of compacted sediments and z_{por} (cm) is the porosity depth attenuation coefficient. These parameters were determined from the measured data at each station (Table S2).

Sediment compaction was considered by allowing the sediment burial velocity to decrease with sediment depth:

$$v_s(x)=\frac{\omega_{acc}\cdot(1-\varphi(L))}{1-\varphi(x)} \quad (3)$$

where ω_{acc} corresponds to the sediment accumulation rate of compacted sediments.

BGD
11, 13067–13126, 2014

The decrease in bioturbation intensity with depth was described with a Gaussian-type function (Boudreau, 1996):

$$D_B(x) = D_B(0) \cdot \exp\left(-\frac{x^2}{2 \cdot x_s^2}\right) \quad (4)$$

where D_B (0) ($cm^2\,yr^{-1}$) is the bioturbation coefficient at the sediment–water interface and x_s (cm) is the bioturbation halving depth.

The flux continuity at the sediment surface serves as the upper boundary condition:

$$F(0) = (1 - \varphi(0)) \cdot \rho \cdot \left(v_s(0) \cdot {}^{210}Pb_{xs}(0) \cdot D_B(0) \cdot \left.\frac{\partial {}^{210}Pb_{xs}(x)}{\partial x}\right|_0\right) \quad (5)$$

where $F(0)$ is the steady-state flux of $^{210}Pb_{xs}$ to the sediment surface ($Bq\,cm^{-2}\,yr^{-1}$). The influx of $^{210}Pb_{xs}$ was determined from the measured integrated activity of $^{210}Pb_{xs}$ multiplied by λ:

$$F(0) = \lambda \cdot \rho \int_0^\infty {}^{210}Pb_{xs}(x) \cdot (1 - \varphi(x))\,dx \quad (6)$$

$^{210}Pb_{xs}$ was present down to the bottom of the core at the 74 m station (12° S), implying rapid burial rates. Here, $F(0)$ was adjusted until a fit to the data was obtained.

A zero gradient (Neumann) condition was imposed at the lower boundary at 50 cm (100 cm for the shallowest stations at 12° S). At this depth, all $^{210}Pb_{xs}$ will have decayed for the burial rates typical of the Peruvian margin. The model was initialized using low and constant values for $^{210}Pb_{xs}$ in the sediment column. Solutions were obtained using the numerical solver NDSolve in MATHEMATICA 9 with a mass conservation > 99 %.

BGD
11, 13067–13126, 2014

The adjustable parameters (ω_{acc}, $D_B(0)$, x_s) were constrained by fitting the $^{210}Pb_{xs}$ data. The goodness-of-fit was done visually since the sampling resolution and variability in the $^{210}Pb_{xs}$ do not warrant more rigorous statistical approaches. Model sensitivity analysis indicated that ω_{acc} are accurate to within ±20 %. Note, however, that the uncertainty in ω_{acc} due the natural sediment heterogeneity may be equivalent to or larger than this value (Turnewitsch et al., 2000). Unsupported ^{210}Pb measurements were not made at the 101 and 244 m station (12° S) and sedimentation rates here were estimated from adjacent stations. Parameters and boundary conditions for simulating $^{210}Pb_{xs}$ at 12° S are given in Table S2. Results for 11° S are given by Bohlen et al. (2011).

3.5 Diagenetic modeling of POC degradation

A steady-state 1-D numerical reaction–transport model was used to simulate the degradation of POC in surface sediments at all stations. The model developed for 12° S is based on that used to quantify benthic N fluxes at 11° S by Bohlen et al. (2011) with modifications to account for benthic denitrification by foraminifera (Dale et al., unpub. data). The methodology used to constrain the POC degradation rates is the same in both studies. A full description of the model can be found in those publications.

The basic model framework follows Eq. (1) i.e. simulating the distribution of dissolved and solid components by considering transport pathways and reactions. Solutes were transported by molecular diffusion and sediment accumulation (burial). Solids were transported by burial and bioturbation, taken from the $^{210}Pb_{xs}$ model. Non-local transport rates of solutes by burrowing organisms (bioirrigation) were very low yet included nonetheless. Solutes simulated include O_2, NO_3^-, NO_2^-, NH_4^+, N_2, H_2S, SO_4^{2-}, Fe^{2+}, DIC and methane (CH_4). Solids include POC, PON, adsorbed NH_4^+, reactive iron (oxy-hydr)oxides and total particulate sulfur. Porewater TA concentrations were not modeled explicitly but calculated from the steady-state porewater concentrations of other ions

BGD
11, 13067–13126, 2014

using the explicit conservative expression (Wolf-Gladrow et al., 2007), as described in Bohlen et al. (2011).

The model includes a comprehensive set of redox reactions that are ultimately driven by POC mineralization. POC was degraded by aerobic respiration, denitrification, iron oxide reduction, sulfate reduction and methanogenesis. Manganese oxide reduction was not considered due to negligible total manganese in the sediment (Böning et al., 2004; Bohlen et al., 2011). The rate of each carbon degradation pathway was determined using Michaelis–Menten kinetics based on traditional approaches (e.g. Boudreau, 1996). DIC is produced by POC degradation only, that is, no carbonate dissolution and precipitation (see Sect. 4).

The total rate of POC degradation was constrained using a novel N-centric approach based on the relative rates of transport and reactions that produce/consume NH_4^+. The procedure follows a set of guidelines that is outlined fully in Bohlen et al. (2011). The modeled POC mineralization rates for 11° S were constrained using both porewater concentration data and in situ flux measurements of NO_3^-, NO_2^- and NH_4^+. Dissolved O_2 flux data were used as an additional constraint at the deeper stations. The POC degradation rates at 12° S were further constrained from the measured DIC and N_2 fluxes. The model output includes concentration profiles, benthic fluxes and reaction rates which are assumed to be in steady-state. Note, however, that the bottom waters on the inner shelf were temporarily depleted in NO_3^- and NO_2^- at the time of sampling due a trapped body of water close to the coast. Although this leads to uncertainties in the rate of nitrate uptake by *Thioploca*, POC degradation rates remain well-constrained from the DIC fluxes.

The model was solved in the same way as described for $^{210}Pb_{xs}$. The sediment depth was discretized over an interval ranging from 50 to 100 cm depending on the station (Boudreau, 1996). Measured solute concentrations and known or estimated particulate fluxes to the sea floor served as upper boundary conditions (Bohlen et al., 2011). At the lower boundary, a Neumann (zero flux) boundary was generally implemented. A steady-state solution was obtained (invariable concentrations with time and sediment

BGD
11, 13067–13126, 2014

depth) with a mass conservation > 99 %. The importance of time-variable boundary conditions is discussed below.

3.6 Pelagic modeling of primary production

Primary production was estimated using the high-resolution physical-biogeochemical model (ROMS-BioEBUS) in a configuration developed for the Eastern Tropical Pacific (Montes et al., 2014). ROMS-BioEBUS consists of a hydrodynamic model ROMS (Regional Ocean Model System; Shchepetkin and McWilliams, 2003) coupled with the **BIO**geochemical model developed for the **E**astern **B**oundary **U**pwelling **S**ystems (BioEBUS, Gutknecht et al., 2013). BioEBUS describes the pelagic distribution of O_2 and the nitrogen cycle with twelve compartments: phytoplankton and zooplankton split into small (flagellates and ciliates, respectively) and large (diatoms and copepods, respectively) organisms as well as detritus, dissolved inorganic N (NO_3^-, NO_2^-, and NH_4^+), dissolved organic N (DON) and a parameterization to determine nitrous oxide (N_2O) production (Suntharalingam et al., 2000, 2012). N cycling under a range of redox conditions is simulated (e.g. Yakushev et al., 2007).

The model configuration covers the region between 4° N and 20° S and from 90° W to the west coast of South America. The model horizontal resolution is 1/9° (ca. 12 km) and has 32 vertical levels that are elongated toward the surface to provide a better representation of shelf processes. The model was forced by heat and freshwater fluxes derived from COADS ocean surface monthly climatology (Da Silva et al., 1994) and by the monthly wind stress climatology computed from QuikSCAT satellite scatterometer data (Liu et al., 1998). The three open boundary conditions (northern, western and southern) for the dynamic variables (temperature, salinity and velocity fields) were extracted from the Simple Ocean Data Assimilation (SODA) reanalysis (Carton and Giese, 2008). Initial and boundary conditions for biogeochemical variables were extracted from the CSIRO Atlas of Regional Seas (CARS 2009, http://www.cmar.csiro.au/cars; for NO_3^- and O_2) and SeaWiFS (O'Reilly et al., 2000; for chlorophyll *a*). Other biogeochemical variables were computed following Gutknecht et al. (2013) and Montes et al. (2014).

BGD
11, 13067–13126, 2014

Monthly chlorophyll climatology from SeaWIFS (Sea-Viewing Wide-Field Sensor) was used to generate phytoplankton concentrations which were then extrapolated vertically from the surface values using the parameterization of Morel and Berthon (1989). Based on Koné et al. (2005), a cross-shore profile following in situ observations was applied to the zooplankton with increasing concentrations onshore.

The simulation was performed over an 18 year period. The first 13 years were run considering only the physics and then the biogeochemical model was coupled for the following five years. The coupled model reached a statistical equilibrium after four years. The data presented here correspond to the final simulation year 18. Details of model configuration and validation are described by Montes et al. (2014).

For this study, we calculated the primary production (PP) integrated over the euphotic zone at the station locations listed in Table 1 for 11° S and 12° S. PP (in N units) was computed as the sum of the new production supported by NO_3^- and NO_2^- uptake and the regenerated production of NH_4^+ uptake by nano- and microphytoplankton (Gutknetch et al., 2013). The atomic Redfield C : N ratio (106/16, Redfield et al., 1963) was used to convert PP into carbon units.

4 Results

4.1 Sediment appearance

Bottom sediments at 12° S were very similar to those at 11° S (see Sect. 2). The sediments down to ca. 300 m were typical cohesive, dark-olive anoxic muds found on the shelf and upper slope (Gutiérrez et al., 2009; Bohlen et al., 2011; Mosch et al., 2012). Porewater had a strong sulfidic odor, especially in the deeper layers. Shelf and OMZ sediments were colonized by mats of large filamentous bacteria, presumably *Thioploca* spp. (Gallardo, 1977; Henrichs and Farrington, 1984; Arntz et al., 1991). Surface coverage by bacterial mats was 100 % on the shelf and decreased to roughly 40 % by 300 m where the bacteria formed patches several decimeters in diameter. Mat density

BGD
11, 13067–13126, 2014

was much lower at 11° S, not exceeding 10 % coverage (Mosch et al., 2012). *Thioploca* trichomes extended 2 cm into the overlying water to access bottom water NO_3^- (cf. Huettel et al., 1996) and were visible down to a depth of ca. 20 cm at the mat stations. Despite anoxic bottom waters, no mats were visible at St. 8 (409 m, 12° S). Sediments here consisted of hard grey clay underlying a 2–3 cm porous surface layer that was interspersed with cm-sized phosphorite nodules. The upper layer contained large numbers of live foraminifera that were visible to the naked eye (J. Cardich et al., unpub. data). Similar foraminiferal "sands" were noted at 11° S, in particular below the OMZ. Phosphorite sands on the Peruvian margin are found where enhanced sediment reworking and winnowing takes place due to dissipation of internal wave energy on the seafloor (Suess, 1981; Glenn and Arthur, 1988; Mosch et al., 2012).

4.2 Sediment mixing and accumulation rates

At most stations, $^{210}Pb_{xs}$ distributions decreased quasi-exponentially and showed little evidence of intense, deep mixing by bioturbation (Fig. 2 and Bohlen et al., 2011); a feature that is supported by the lack of large bioturbating organisms in and below the OMZ (Mosch et al., 2012). The highest bioturbation coefficient determined by the model was 4 $cm^2\,yr^{-1}$ for St. 3 at 12° S (Table S2). Because megafauna were absent during fieldwork, the non-zero mixing rates probably reflect the intermittent colonization by fauna that takes place during periodic oxygenation events (Gutiérrez et al., 2008).

Mass accumulation rates derived from $^{210}Pb_{xs}$ modeling were similar to values reported previously (Reimers and Suess, 1983c). Rates were extremely high at the shallowest stations (1200 and 1800 g $m^{-2}\,yr^{-1}$ at 11 and 12° S, respectively); a factor of 2–3 times higher than measured elsewhere on the transects and 3–4 times higher than the global shelf average of 500 g $m^{-2}\,yr^{-1}$ (Burwicz et al., 2011). They corresponded to sedimentation rates of 0.45 and 0.3 cm yr^{-1} (Table 2). Beyond the inner shelf, the sedimentation rates (ω_{acc}) showed much more variability at 12° S than at 11° S, although this could be due to the higher sampling resolution along 12° S. Relatively low mass

BGD
11, 13067–13126, 2014

accumulation rates of 44 g m^{-2} yr^{-1} were calculated for St. 8 at 12° S where erosion occurs.

4.3 Geochemistry

Dissolved O_2 concentrations in the water column reveal the vertical extent of the OMZ and the presence of oxygen-deficient water overlying the upper slope sediments at both latitudes (Fig. 1). Qualitatively, geochemical solute profiles from 11 and 12° S are typical for continental margin settings (Bohlen et al., 2011; Fig. 3). Sediment porewater concentrations of NH_4^+ and alkalinity were highest on the shelf and decreased with water depth. Conversely, SO_4^{2-} depletion was more extensive at the shallower stations. SO_4^{2-} also showed a much stronger depletion on the shelf at 12° S compared to 11° S, leading to the formation of a methanogenic layer below 65 cm. The model was able to accurately simulate the geochemical profiles along both transects at all stations (Fig. 3 and Bohlen et al., 2011).

Sulfate reduction is the dominant organic matter (OM) respiration pathway throughout and below the OMZ (Bohlen et al., 2011). The above trends in porewater concentrations thus confirm general expectations that less reactive organic material reaches the sea floor as water depth increases (e.g. Suess, 1980; Levin et al., 2002). Indeed, measured DIC fluxes and model results provide independent support for decreasing POC degradation rates with distance offshore (see Sect. 4.5). The decrease in free sulfide in the deeper sediment layers with increasing water depth also fits with this idea. However, sulfide oxidation by *Thioploca* overprints any obvious relationship between sulfide accumulation and OM degradation in the upper 20 cm of sediments (Henrichs and Farrington, 1984; Bohlen et al., 2011).

4.4 Organic carbon distributions

Surface POC content at 12° S was lowest (ca. 5 %) on the inner shelf and below the OMZ (Fig. 3). POC decreased in the upper 5 cm and remained constant thereafter.

BGD
11, 13067–13126, 2014

PON showed the same qualitative trends. Maximum POC contents of ca. 17 % were measured inside the OMZ and are typical for the Peruvian margin (Suess, 1981). The relatively low POC content on the inner shelf is somewhat anomalous since one may have expected highest values at the shallowest water depths given the higher primary production (see below) and shorter transit time for organic detritus to reach the seafloor. At the OMZ sites, POC showed a marked change at around 15 to 20 cm depth (Fig. 3) which may reflect the regime shift in the Peruvian OMZ during the little ice age circa 1820 AD postulated by Gutiérrez et al. (2009). These features were also present at the St. 4 and 5 on the outer shelf. The steady-state model does not capture centennial changes in OMZ conditions suggested by the POC profiles. Very similar trends were observed at 11° S, implying that OM distributions are qualitatively and quantitatively driven by the same first-order processes at both latitudes.

4.5 DIC fluxes

The modeled DIC concentrations inside the benthic chambers at 12° S showed good agreement with those calculated from measured TA and pCO_2 concentrations (Fig. 4 and Table S1). Measured and modeled fluxes agreed to within ±50 %, but most stations were simulated to within ±20 % or better (Fig. 5a). It should be remembered that the model is not only constrained by the DIC fluxes but also by porewater distributions and benthic DIN and O_2 fluxes (Bohlen et al., 2011). Thus, whilst the modeled DIC fluxes could be improved, they form only one aspect of the overall goodness-of-fit to the observed database. In general, the agreement between the modeled and measured DIC fluxes affords confidence in the modeled DIC fluxes at 11° S where in situ pCO_2 measurements were not made (Table 2).

Measured DIC fluxes were high on the inner shelf (65.9 mmol m^{-2} d^{-1}) and decreased quasi-exponentially with depth (Table 2). DIC fluxes were low in the OMZ at 12° S (2.2–4.7 mmol m^{-2} d^{-1}) and similar to the deep sites (1.2–2.8 mmol m^{-2} d^{-1}). The DIC fluxes at 11° S showed the same trends, although the flux on the inner shelf (8.2 mmol m^{-2} d^{-1}) was a factor of 8 smaller than at 12° S.

BGD
11, 13067–13126, 2014

DIC was assumed to originate entirely from POC mineralization. There was no clear increase or decrease in Ca^{2+} and Mg^{2+} concentration in the benthic chambers that would indicate an important role for carbonate precipitation/dissolution (data not shown). This is also inferred from porewater gradients of Ca^{2+} and Mg^{2+} at 12° S (Fig. S3). Fluxes calculated from the gradients show that the potential contribution of carbonate precipitation was < 5 % of the DIC flux across all stations. This is well within the error of the DIC flux (Table 2), such that carbonate precipitation can be ignored for all practical purposes.

4.6 Organic carbon burial efficiency (CBE)

CBE (%) was calculated using the POC accumulation rates and DIC fluxes, i.e. CBE = POC accumulation rate/(POC accumulation rate + DIC flux) × 100 % (Table 2). CBE is a subjective metric since it depends on the chosen depth where one considers that OM degradation no longer occurs to a significant degree. At the inner shelf and deep stations, POC reaches asymptotic values at around 10 cm (Fig. 3) where organic material is relatively refractive (Reimers and Suess, 1983a). CBE was thus calculated at this depth for these stations. At the OMZ stations, due to variations in POC content in the upper 10 cm, the average POC content in the upper 10 cm was used in the calculations. For St. 8 at 12° S (409 m), CBE was calculated at 3 cm since the underlying sediment was old, non-accumulating clay.

We quantified the uncertainty in the CBE calculation based on a 20 % error in ω_{acc} and POC content and the difference in DIC fluxes measured simultaneously in two chambers during each lander deployment (Table 2). The latter arises from the natural "patchiness" of the seafloor and is much greater than the combined analytical error in the TA and pCO_2 measurements. Errors due to artifacts leading from the enclosure of bottom water by landers are likely to be small (e.g. Hinga et al., 1979). On average, the relative error in DIC flux is the same as that for the POC accumulation rate, around 30 % (Table 2). This leads to a mean relative error in CBE across all stations (at 12° S) of around 40 %.

BGD
11, 13067–13126, 2014

Measured and modeled CBE show very good agreement (Fig. 5b). CBE at 12° S was lowest on the inner shelf (< 20 %). This contrasts with the organic carbon accumulation rate which was actually highest here (60 g m^{-2} yr^{-1}; Table 2). Low CBE of 19 ± 6 % were also observed at the 409 m site due to the low sediment accumulation rate. The highest CBE was calculated for St. 5 (74 ± 37 %). At 11° S the modeled range of CBE was very similar yet with a higher shelf value (47 %, Table 2). The maximum CBE of 81 % was calculated for the 695 m station below the OMZ.

4.7 Primary production (PP) and organic carbon rain rate

PP estimates from the ROMS-BioEBUS model for 11 and 12° S are shown in Fig. 6. With the exception of the shallowest station, the data represent the annual mean ± s.d. for the locations where BIGO landers were deployed. There were no large differences in PP between the two latitudes and or across the OMZ. For instance, PP increased from only ca. 80 mmol m^{-2} d^{-1} at the deepest point to ca. 110 mmol m^{-2} d^{-1} at the shallowest. However, the model revealed a much larger intra-annual variability ranging from ca. 70 to 170 mmol m^{-2} d^{-1} with highest values in austral summer (see Fig. S2). PP was dominated by diatoms at both latitudes.

Organic carbon rain rates to the seafloor (RRPOC) were calculated as the sum of the benthic carbon oxidation rate (i.e. DIC flux) and the accumulation rate at 10 cm (Table 2). RRPOC showed a rapid decrease on the shelf stations at 12° S with a more attenuated decrease with depth (Fig. 6a). Station 8 (409 m) at 12° S is again an exception due to the low POC accumulation there. At 11° S the trends were not so obvious due to fewer sampling stations (Fig. 6b). The fraction of PP reaching the sediment in the OMZ and deep stations was < 1 to 12 % for both transects (Fig. 6c).

BGD
11, 13067–13126, 2014

5 Discussion

5.1 Carbon mineralization in the water column

A comparison of the rain rates and PP estimates from the ROMS-BioEBUS model shows that only a minor fraction of PP reaches the seafloor. The true fraction may be even lower since modeled PP is 2 to 3 times lower than the range of 250 to 400 mmol m^{-2} d^{-1} reported previously (Walsh, 1981; Quiñones et al., 2010 and references therein). This underestimation may be due to the coarse model spatial resolution (1/9°) which cannot accurately resolve nearshore processes. The model also represents climatological conditions (i.e. annual mean state), whereas PP measurements made during neutral or cold ENSO phases (i.e. La Niña) are likely to higher than the long-term mean (Ryan et al., 2006). The rate at which OM is respired during transit through the water column is usually calculated using sediment trap data (Martin et al., 1987). The decrease in the sinking flux, $F(z)$, has been widely described using the following function:

$$F(z) = F_{100} \cdot (z/100)^{-b} \quad (7)$$

where F_{100} is the flux at 100 m, z (m) is water depth and b is the dimensionless attenuation coefficient (Martin et al., 1987). A mean b value of 0.86 for oxic open-ocean waters was derived from the VERTEX program (Martin et al., 1987) and such values are routinely used in global biogeochemical models (e.g. Dunne et al., 2007). b values lower than 0.86 indicate a slower rate of degradation compared to the mean value and vice-versa.

In the absence of sediment trap data, we estimated b for the Peruvian transects by fitting the modeled rain rates to the following function analogous to Eq. (7):

$$\mathrm{RRPOC}(z) = \mathrm{RRPOC}_{101} \cdot (z/101)^{-b} \quad (8)$$

To facilitate comparisons with other studies, the rain rate at the 101 m station at 12° S was taken as the reference flux. Pooling the data ≥ 101 m from both transects (Fig. 7),

BGD
11, 13067–13126, 2014

and excluding the data from St. 8 which is affected by erosion, the best fit to Eq. (8) is obtained with $RRPOC_{101} = 28.9 \pm 3.2\,mmol\,m^{-2}\,d^{-1}$ and $b = 0.88 \pm 0.17$ (NonlinearModelFit function in MATHEMATICA). The low derived export flux compared to PP rates confirms previous results that most PP in the Humboldt system is mineralized in the surface mixed layer under "normal", i.e. non-El-Niño, conditions (Walsh, 1981; Gagosian et al., 1983; Quiñones et al., 2010 and references therein).

Our derived *b* coefficient for the Peruvian OMZ is indistinguishable from the mean value derived by Martin et al. (1987) for normal oxic waters (Fig. 7). Yet, several studies have shown that respiration of OM in the water column is significantly reduced by the absence of O_2, leading to elevated carbon fluxes to the lower water column and sediments (Martin et al., 1987; Devol and Hartnett, 2001; Van Mooy et al., 2002). For example, a coefficient of 0.32 was determined by Martin et al. (1987) for a station 60 km offshore Peru at 15° S within the OMZ. Similarly low coefficients (0.36–0.40) have been reported for the oxygen-deficient Mexican margin (Devol and Hartnett, 2001; Van Mooy et al., 2002), but not for the Arabian Sea OMZ (0.79 ± 0.11; Berelson, 2001). Van Mooy et al. (2002) supported their findings with laboratory experiments showing that natural particulate material collected at the base of the euphotic zone was degraded less efficiently under anoxic vs. oxic incubation conditions. Given the anoxic water mass residing on the Peruvian margin, therefore, a much lower *b* coefficient may have been expected.

Devol and Hartnett (2001) observed that rain rates to the seafloor on the Mexican margin, calculated using benthic carbon oxidation rates and burial fluxes at nine stations, showed a very good agreement with sediment-trap estimates. Although some variability in *b* within a given oceanic region is to be expected (Berelson, 2001), the large difference between our calculated *b* value and those previously derived for Peru and Mexico is enigmatic. Van Mooy et al. (2002) proposed that a lack of zooplankton at Mexico may reduce the pre-processing and packaging of OM prior to export, favoring preferential preservation of sinking OM. This hypothesis was recently confirmed by Giering et al. (2014) at a normal oxic site in the North Atlantic. They demonstrated

BGD
11, 13067–13126, 2014

that zooplankton mediate the disaggregation of large organic particulates into slowly-sinking material that is subsequently mineralized by microorganisms. Zooplankton-bacteria interactions may be similarly instrumental in OM breakdown at Peru (this study), although sufficient data is currently lacking to support this idea (Ayón et al., 2008). Further south offshore Chile, high mineralization rates were indeed linked to a very efficient microbial loop that was closely associated with nanozooplankton assemblages (Bottjer and Morales, 2005; Levipan et al., 2007).

Microbial communities adapted to depressed O_2 levels are also very active metabolically in the underlying OMZ at Peru (Lam et al., 2009; Kalvelage et al., 2013). High rates of aerobic heterotrophic respiration have been measured where dissolved O_2 concentrations are in the sub-micromolar range and thus far lower than the detection limit of the Winkler assay (Kalvelage et al., 2013). Even though O_2 is not detectable, it may nonetheless be transported from the surface ocean to the OMZ interior by diapycnal mixing and rapidly consumed. For instance, diapycnal mixing along the upper continental slope and the lower shelf region of the Mauritanian upwelling supplies around 80 mmol m^{-2} d^{-1} to the underlying oxygen-deficient waters (Brandt et al., 2014). This exceeds the benthic oxygen uptake by about a factor of 8 (Dale et al., 2014), implying that most of it is consumed in the water column. This mixing also operates on the Peruvian margin and is strongly enhanced due to presence of non-linear internal waves (M. Dengler, unpub. data). A different interplay between physical mixing processes and microbial community respiration may well operate at the offshore station at 15° S where low *b* values were determined.

Multi-decadal oscillations in oceanographic conditions may modify particle fluxes in different ways. Martin et al. (1987) conducted their Peru fieldwork in June 1983 which coincided with a positive El Niño index, that is, a warm phase (http://www.cpc.ncep.noaa.gov). This contrasts with the neutral conditions encountered on our surveys of 11° S and 12° S. It is well documented that strong ENSO events alter the ecosystem functioning off Peru, and sub-mesoscale zooplankton and anchoveta (*Engraulis ringens*) distributions are often dictated by the upwelling intensity (Jordán, 1971; Bertrand

BGD
11, 13067–13126, 2014

et al., 2008; Tam et al., 2008). The relative contribution of zooplankton and anchoveta fecal pellets to total carbon export flux is thus expected to vary widely in time and space (Walsh, 1981; Staresinic et al., 1983). This may be of relevance because sinking speeds of zooplankton and anchoveta fecal pellets are very different, the latter being 10 times higher at around 1000 m d^{-1} (Staresinic et al., 1983). It should be noted that anchoveta abundance has also undergone large fluctuations in recent decades, with total landings being less than 2×10^6 t in the early 1980s (i.e. during Martin et al.'s (1987) fieldwork) to more than 10×10^6 t in the 2000s (http://www.fao.org). Zooplankton biomass has undergone similar variations, and the two are probably linked (Ayón et al., 2008).

There may be other explanations that contribute to the regional differences in *b* values related to the approaches used to calculate *b*. "Bottom-up" (i.e. using sediment DIC fluxes and POC burial rates) and "top-down" (e.g. sediment traps) approaches integrate carbon fluxes over very different time-scales and each suffer from their own unique uncertainties. For instance, sediment traps may underestimate the particle flux in water depths < 1500 m due to high lateral current velocities (Yu et al., 2001); an effect likely to be exacerbated on shallower margins (Jahnke et al., 1990). Furthermore, data from a single trap deployment will only capture the settling flux on time-scales similar to the deployment time. The particle flux measured at 15° S will thus be biased towards the productivity and particle dynamics during the eight day period that the trap was operational (Martin et al., 1987). This should raise concerns because PP at 15° S shows high temporal variability (Walsh et al., 1981) and the low *b* coefficient there may be spurious. Particle fluxes in the Arabian Sea also experience high variability due to monsoonal forcing (Haake et al., 1992), and may explain why Berelson (2001) reported similar *b* coefficients to ours for the Arabian Sea instead of lower values. The issue of temporal variability in benthic fluxes is dealt with separately in Sect. 5.4.

Finally, rain rates to the seafloor could be systematically higher than suggested by our data if sediment particles are resuspended and transported down-slope (laterally) in a benthic nepheloid layer (Jahnke et al., 1990). In this case, the measured *b* co-

BGD
11, 13067–13126, 2014

efficient determined from benthic data would be reduced relative to values calculated from sediment trap data. However, for this explanation to hold, it would require sediment resuspension in an exponential-like fashion with increasing water depth (Fig. 7). Yet, sediment winnowing and erosion on the margin occurs in discrete depth intervals due to the dissipation of internal waves with the seafloor, as reflected in the low POC accumulation rate at St. 8 at 12° S (Reimers and Suess, 1983b; Arthur and Dean, 1998; Mosch et al., 2012). Whilst it seems unlikely that sediment resuspension and lateral export can wholly explain the low rain rates along both transects, the redistribution of old, reworked material downslope may have important implications for the carbon burial efficiency in sediments below the OMZ (see Sect. 5.3.4).

5.2 Carbon burial and preservation across the margin

Although questions remain regarding the efficiency of OM mineralization in the water column, it seems clear the sediments at 11 and 12° S play a rather minor role in the regional carbon cycle. Because inorganic carbon is not limiting to phytoplankton, the significance of the benthic carbon cycle lies instead with the fraction that is permanently buried. On very long time scales, burial of carbon in marginal sediments represents a net removal of CO_2 from the atmosphere and a net source of atmospheric O_2 (Berner, 1982). Muddy continental margin sediments in the modern ocean (< 1000 m) account for 70–85 % of global carbon burial, despite covering < 10 % of the seafloor (Hedges and Keil, 1995; Burdige, 2007). On an areal basis, mean POC burial on the continental margin is 0.5–1.1 mmol C m^{-2} d^{-1}, compared to only < 0.05 mmol C m^{-2} d^{-1} in the deep sea (Table 3). Oxygen-poor marine environments along ocean margins are believed to be even more important hotspots of carbon burial and candidate sites for petroleum-source rock formation (Demaison and Moore, 1980).

To place the Peruvian margin in this context, the cumulative POC burial is first plotted against water depth in Fig. 8b. This was calculated by integrating the measured POC accumulation at each station in Table 2 over the distance between stations in Fig. 8a. The trends at 11 and 12° S are not identical despite both transects being located within

BGD
11, 13067–13126, 2014

the same upwelling cell (Quiñones et al., 2010). POC burial increases rapidly on the inner shelf to ca. 100 m at both latitudes, at which point the rates of increase diverge to give higher burial at 12° S down to the lower edge of the OMZ. Burial at 11° S then takes over as the primary site of POC preservation, reaching a grand total of 254 kmol C m^{-1} yr^{-1} (per meter of coastline). A lower value of 181 kmol C m^{-1} yr^{-1} was calculated for 12° S. Possibly, the formation of coastal eddies at 12° S exports a greater fraction of particulate matter offshore compared to 11° S (Stramma et al., 2013).

Mean POC burial on the margin, calculated by dividing the total cumulative burial by the transect length, is between 6.1 and 6.8 mmol C m^{-2} d^{-1}, which is 2–5 times higher than the global margin average of 1.4–2.9 mmol C m^{-2} d^{-1} (Table 3). A similar calculation can be made on the basis of CBE. Using the distances in Fig. 8a and CBE from Table 2, the mean CBE for the 11° S and 12° S transects is 51 and 58 %, respectively. These are much higher than the global average of 30 % for muddy marginal sediments (Burdige, 2007). In view of the fact that the fraction of exported OM that reaches the sediment at these latitudes is the same as for normal oxic waters (same *b* value), this result demonstrates that carbon is being preferentially sequestered and preserved in sediments compared to the average continental margin. An understanding of the factors that drive carbon preservation on the Peruvian margin may thus help to determine benthic-pelagic feedbacks in both the ancient and future ocean and the reasons for POC concentration changes in the sedimentary record.

5.3 Controls on organic carbon preservation

5.3.1 Significance of O_2

Figure 9 shows that the CBE depends on sedimentation rate for a range of marine environments with differing bottom water O_2 concentrations (Müller and Suess, 1979; Henrichs and Reeburgh, 1987; Betts and Holland, 1991; Canfield, 1993; Aller, 1998; Burdige, 2007). This dependency arises because sediment accumulation is intrinsically linked to carbon burial flux, which itself is strongly tied to rain rate (Müller and Suess,

BGD
11, 13067–13126, 2014

1979). Sediments underlying oxygen deficient waters appear to have a higher CBE. Yet, the CBE in sediments above and below the OMZ at Peru shows unexpected trends compared to the existing database. Firstly, the CBE data for the anoxic inner shelves where sedimentation rates and rain rates are highest (blue stars) plot within the range for normal oxic conditions vs. expected values of > 50 % for oxygen-poor conditions. Secondly, sediments underlying oxygen-containing bottom waters below the OMZ have a higher-than-expected CBE of up to 81 % (green stars) and plot alongside those from oxygen-deficient and euxinic waters.

The significance of bottom water O_2 in this plot remains ambiguous after several decades of discussion (Demaison and Moore, 1980; Pedersen and Calvert, 1990; Canfield, 1993; Hedges and Keil, 1995; Zonneveld et al., 2007). On the one hand, some workers have argued that there is no clear effect of bottom water O_2 on CBE (Pedersen and Calvert, 1990; Burdige, 2007; Flögel et al., 2011). This observation is supported by sediment manipulation experiments showing that labile OM is readily degraded under both oxic and anoxic conditions (Otsuki and Hanya, 1972; Westrich and Berner, 1984). On the other hand, Canfield (1993, 1994) argued in favor of enhanced preservation under low O_2 (< 20 µM) for mass accumulation rates $< 0.1\,g\,cm^{-2}\,yr^{-1}$. Interestingly, most stations on the outer shelf and OMZ fall into this category. Supporting experimental evidence is provided by studies showing that the degradation of refractive OM occurs only in the presence of O_2, possibly because strong oxidants such as peroxide are required (e.g. Hedges and Keil, 1995; Hulthe et al., 1998). Similarly, Reimers and Suess (1983a, b) attributed OM preservation in the Peruvian OMZ to limited exposure to O_2 prior to burial and the formation of insoluble humin termed "proto-kerogen".

Whilst empirical relationships like Fig. 9 are informative for comparative purposes, they do not provide any understanding on the mechanisms of carbon preservation. Besides, it has long been recognized that bottom water O_2 concentration per se is not the correct metric for proper interpretation of CBE (Hedges and Keil, 1995; Hedges et al., 1999; Meile and Van Cappellen, 2005). OM preservation may proceed directly by the production of (i) refractory molecules via abiotic condensation reactions and (ii)

BGD
11, 13067–13126, 2014

hydrolysis-resistant, biologically refractive macromolecules by microorganisms. Indirect preservation, that is, inhibition of mineralization, includes factors such as physical protection of OM by minerals and processes linked to O_2 availability. These factors have been discussed extensively already and it is not our intention to repeat them here (Hedges and Keil, 1995; Burdige, 2007; Zonneveld et al., 2007). Instead, we seek a plausible explanation for the factors that contribute to trends in Fig. 9, basing our discussion on the specific environmental characteristics of the Peruvian margin between 11 and 12° S.

5.3.2 Sorptive preservation

Mineralization of OM begins with hydrolytic and enzymatic attack by microorganisms (Arnosti, 2004). The rate of this process may be reduced if OM becomes shielded from exoenzymes by interacting with small pores on the surface of fine-grained inorganic particles (Keil et al., 1994; Mayer, 1994; Coppola et al., 2007). The premise is that physical protection is afforded by size and steric constraints of the mesopores that become infiltrated with the organic molecules (Mayer, 1994). At a fundamental level, one could thus infer from our derived CBEs that there are large differences in grain size along the transects. Indeed, such differences do exist, but contrary to expectations the clay and silt fractions are higher, not lower, on the shelf with increasing sand content down slope (Mosch et al., 2012). Hence, there must be additional factors at work which are more significant in reducing CBE on the inner shelf than grain size effects are at increasing CBE. Conversely, identical or different factors must favor carbon preservation at the deeper sites, despite the overall increase in grain size.

One explanation could be related to the sorptive capacity of OM in fine-grained organic-rich sediments. This is normally quantified as the organic carbon (wt.%) to surface area ratio (OC/SA) (Mayer, 1994). In the quasi-permanently anoxic OMZ sediments, super-monolayer coatings (OC/SA > 2–5) may dominate over the monolayer equivalents that characterize normal continental margin sediments (Keil and Cowie, 1999). Hedges and Keil (1995) suggest, among other reasons, that super-monolayers

BGD
11, 13067–13126, 2014

result from equilibration with elevated porewater DOC concentrations and possibly high levels of bacterial exopolymers in the case of Peru (Parkes et al., 1993). One could expect higher levels of porewater DOC in the core of the OMZ where POC contents are highest (Fig. 3, Table 2). Burial of this adsorbed material would ultimately favor higher CBEs in the OMZ, especially if the organic coatings are subject to ageing, vulcanization or condensation processes (Hedges and Keil, 1995).

The situation could be quite different on the shelf. Even though the bottom waters were anoxic at the time of sampling, O_2 concentrations can change by several tens of µM within days or weeks (Gutiérrez et al., 2008). These dynamics are driven by seasonal and sub-seasonal anomalies in oceanographic conditions manifested as trapped coastal waves in combination with temporal changes in water column respiration rates. During periods of prolonged oxygenation, the benthic community structure evolves rapidly from being dominated by *Thioploca* mats to macrofauna, triggering changes in vertical mixing, bioirrigation rates and grazing intensities (Tarazona et al., 1988; Gutiérrez et al., 2000). In the long-term, these factors may well improve sediment ventilation and reduce the accumulation of porewater DOC on the shelf compared to the OMZ (Burdige, 2002), leading to lower OC/SA ratios and CBEs. These ideas remain speculative for the moment but could be easily tested in future.

5.3.3 Macrofauna

The impact of macrofauna on OM decomposition has been further summarized by Burdige (2006). A broad conclusion that can be drawn from this and other studies is that macrofaunal activity leads to an overall enhancement of OM mineralization and, hence, a reduction in CBE (Calvert et al., 1992 provide evidence for an alternative view). Burial efficiencies in the Peruvian OMZ are indeed high where large bioturbating macrofauna are permanently absent and bioturbation rates are negligible (Mosch et al., 2012; Table S2). Direct impacts on OM mineralization by animals are caused by grazing and excretion of organic compounds. Indirect effects include transport and fragmentation of OM and sediment ventilation; the latter being a potential link with OC/SA ratios.

BGD
11, 13067–13126, 2014

Episodic colonization of shelf sediments by animals would also create redox oscillations which have been suggested as a fast-track for mineralization of refractive organic compounds via priming or co-oxidation pathways (Aller, 1994; Canfield, 1994; Hulthe et al., 1998).

Koho et al. (2013) also stressed the importance of macrofauna in priming OM in sediments of the Arabian Sea OMZ ($< 22\,\mu M\ O_2$). OM is preferentially preserved here relative to open-ocean areas (Haake et al., 1992). Using diagenetic indicators including the abundance of hydrolysable amino acids and the amino acid degradation index, DI, Koho et al. (2013) identified an enrichment of high-quality reactive OM in the core of the OMZ that was associated with low bulk mineralization rates (Cowie and Hedges, 1994; Dauwe et al., 1999). They explained this apparent paradox as a lack of particle manipulation by macrofauna, basing their ideas on earlier studies (Witte et al., 2003; Burdige, 2006; Vanderwiele et al., 2009; Moodley et al., 2011; Hunter et al., 2012). They concluded that macrofauna catalyze the breakdown of large organic particles into smaller bioavailable substrates. By contrast, mineral sorption (i.e., OC/SA) was ruled out as the dominant factor influencing OM distributions (Vanderwiele et al., 2009).

In agreement with the Arabian Sea studies, biochemical investigations across the Peruvian margin also identified clear differences in amino acid and DI (Niggemann and Schubert, 2006; Lomstein et al., 2009). In a survey of 22 stations between 10 and 14° S, Lomstein et al. (2009) observed that the percentage of total organic carbon and nitrogen attributable to amino acids (an indicator of OM "freshness") was highest on the outer shelf and within the OMZ (ca. 130–360 m). Lower values were reported for the inner shelf and below the OMZ, indicating OM in a great state of degradation. Similarly, the highest DI values (> 1.0) were observed in the OMZ. These findings might be explained by reduced diagenetic alteration of OM at the stations with low or little dissolved O_2 (Levin et al., 2002). OM preservation may, therefore, be controlled by the same first-order factors (possibly related to macrofauna), in both the Arabian Sea and the Peruvian margin. A more robust comparison would benefit from CBE estimates in Arabian Sea sediments.

BGD
11, 13067–13126, 2014

5.3.4 Lateral particle transport

A central assumption behind the CBE calculation is that OM settles vertically through the water to be deposited on the seabed without further mobilization. However, as mentioned earlier, physical resuspension and winnowing of fine-grained biogenic debris will redistribute some OM down-slope (Krissek et al., 1980; Mosch et al., 2012). This would artificially skew CBE upwards at deeper sites, especially if the material is reworked and less reactive (Kim and Burnett, 1988; Jahnke et al., 1990; Arthur and Dean, 1998; Levin et al., 2002). We suggest that this mechanism may partly account for the high CBE observed at the deep oxygenated sites in Fig. 9. A similar proposal was made for the southern California Basins by Berelson et al. (1996). An understanding of the origin and freshness of the OM at the moment it finally settles on the seabed is thus critical to correctly determine the true CBE (Hedges and Keil, 1995).

5.4 Uncertainties

The previous discussion illustrates that the conflicting views on the role of O_2 on OM preservation are not irreconcilable. Factors indirectly related to O_2 can explain the low OM preservation efficiency on the inner shelf as well as the relatively higher burial efficiency in the OMZ stations. However, several aspects related to temporal heterogeneity are worth mentioning because they create uncertainty in the results which is difficult to quantify using the available data.

To begin with, the error in CBE could be larger than calculated (average 40 %) if the POC content that is used to calculate the buried fraction is decoupled (in time) from carbon being respired and released from the seafloor as DIC. The idea is that the POC burial calculation integrates over a much longer time-scale than the instantaneous DIC flux which is more susceptible to short-term (sub-annual) variability. This has clear relevance for the Peruvian margin because of the increase in carbon content, mineralization and burial rates that coincided with the little ice age when the OMZ expanded and de-oxygenation intensified (Gutiérrez et al., 2009). For these centennial

BGD
11, 13067–13126, 2014

time-scales and diffusive path lengths (ca. 10 cm), DIC fluxes will adjust to the higher mineralization rates within a few years only (Lasaga and Holland, 1976). Particle burial fluxes require much longer, roughly $t = \Delta x/\omega_{acc}$ yr, where Δx is the reference depth of carbon burial. For Δx = 10 cm, t = 20 to 900 yr for the range of sedimentation rates on the margin, implying that organic carbon burial in the upper 10 cm at the outer shelf and OMZ stations is still adjusting to the higher rain rates that ensued around 200 years ago (Fig. 3). Nonetheless, since burial accounted for the largest fraction of the rain rate at these sites, on average 55 % with values as high as 74 % at St.5, the sensitivity of CBE to changes in carbon accumulation rate is not dramatic. The regime shift is not recorded at the inner shelf sites because the high sedimentation rates restrict the observable archive to the last 100 years. Similarly, the deep stations below the OMZ are presumably beyond the sphere of influence of short-term climactic variations. Consequently, these sites show instead the expected decrease in POC for sediments undergoing steady-state mineralization with very little mixing by bioturbation (Fig. 3).

Short-term temporal variability in rain rate and DIC fluxes will lead to further error in the CBE (Burdige, 2007; Witte et al., 2003). The relative standard deviation of PP across the transect, which can be taken as measure of intra-annual variability of rain rate, is around 26 %. This is lower than the mean calculated error in CBE yet still non-negligible (see Fig. S2). It could be argued that the overall impact of seasonality in PP is small because it varies more or less incrementally between a maximum in austral summer to a minimum in winter (Fig. S2). Yet, it is currently not possible to infer the extent to which the temporal variability in rain rate adds or subtracts from the uncertainty in CBE. This is a subject that could be tackled by modeling (see below).

The contribution of sulfur oxidizing bacteria to the benthic carbon cycle is unknown. Time-series data from the Peru shelf revealed continuous fluctuation in *Thioploca* biomass by as much as 50 g C m^{-2} within a single year in response to the local availability of bottom water O_2 and NO_3^- (Gutiérrez et al., 2008). Anoxic bag incubations of sediment slurries along the 12° transect revealed that a fraction of porewater DIC was consumed at water depths with a high abundance of *Thioploca* spp. (T. Treude,

BGD
11, 13067–13126, 2014

unpubl.). The time-scale for mineralization of bacterial carbon has not been quantified but is likely to be rapid. Mass balances show that the uptake, storage and release of dissolved N by *Thioploca* on the inner shelf shift the benthic N cycle away from steady-state (Sommer et al., unpub. data).

In order to help resolve these and similar issues, a logical progression would be to simulate benthic fluxes and burial using a model that combines the known kinetics of OM degradation on the margin (Bohlen et al., 2011) with time-varying particle fluxes to the sea floor and bottom water O_2 and NO_3^- (e.g. Dale et al., 2013). This would allow the temporal variability in DIC fluxes to be assessed and help with the design of future sampling programs. Because OM preservation is critical for O_2 and nutrient budgets of the pelagic system, a better description of the temporal variability in benthic carbon burial vs. mineralization is also required to more accurately simulate redox sensitive processes such as denitrification in the water column. This is true not only for the Peruvian margin (Montes et al., 2014) but for the ocean as a whole (Kriest and Oschlies, 2013).

6 Conclusions and outlook

Fieldwork undertaken within the framework of the SFB 754 program has led to an extensive database of new benthic observations on the fascinating Peruvian margin. This has improved our understanding of particulate organic carbon (POC) cycling under low oxygen conditions and expanded considerably the existing database on CBEs in oxygen-deficient environments (Canfield, 1993; Burdige, 2007). Our two key findings are: (1) POC rain rates to the seafloor are not enhanced by low oxygen concentrations in the overlying water column, (2) low oxygen concentrations in ambient bottom waters promote the preservation of POC in sediments. Being the most productive region in the world with a large expanse of anoxic water impinging the seafloor, the Peruvian upwelling is perfectly suited to study the effects of oxygen on POC turnover in an open margin setting. The following have been identified as key outstanding questions:

BGD
11, 13067–13126, 2014

– Future research should attempt to better quantify the POC respiration rate in the water column, with particular focus on the efficiency of the microbial loop, particulate composition (organic and inorganic), sinking rates and the importance of zooplankton vs. anchoveta fecal pellets. Why is mineralization of organic matter in the water column at 11 and 12° S Peru apparently so much more efficient compared to 15° S (Martin et al., 1997) and other oxygen-deficient regions such as the Mexican margin? Is there a significant transport of O_2 into the OMZ interior by diapycnal mixing as observed on the Mauritanian margin? Or is there a significant down-slope export of particulate material in the benthic boundary layer?

– The sediments are extremely enriched in POC, yet the factors controlling its preservation are imperfectly understood. Quantifying the role of animals (bioturbation, bioirrigation) will be difficult in the long-term given their uneven distribution in time and space. Yet, biochemical indicators of organic matter quality, such as amino acid distributions, could be easily measured to aid the interpretation of carbon burial efficiencies. In general, the cycling of dissolved organic matter cycling in sediment porewaters in Peruvian sediments is poorly known. How much of the total carbon pool is dissolved and returned to the water column, and what is its relation to carbon content and mineral surface area? To what extent are the dissolved organic C, N and P cycles coupled/uncoupled and is there any regulation by *Thioploca*?

– The temporal variability of benthic mineralization and corresponding uptake of bottom water O_2 and NO_3^- requires urgent attention. The Peruvian shelf is a highly dynamic environment where non-steady-state conditions are common. Pre-existing steady-state benthic models need to assimilate long-term observational data including *Thioploca* biomass (e.g. Gutiérrez et al., 2008) in order to better predict long-term benthic-pelagic coupling. This is especially important for N, P and Fe fluxes from the sediments that are amongst the highest ever reported (Bohlen et al., 2011; Noffke et al., 2011; Scholz et al., 2011). Furthermore, an accurate

BGD
11, 13067–13126, 2014

description of nutrient fluxes, as well as carbon burial, should be implemented in regional models such as ROMS-BioEBUS. The contribution of sediments on the Peruvian margin to primary production on short (e.g. days, weeks) and long (e.g. months, years) time-scales is completely unknown at this time.

The Supplement related to this article is available online at doi:10.5194/bgd-11-13067-2014-supplement.

Acknowledgements. We thank the captains and crew of RV *Meteor* cruises M77 and M92 for their assistance during the fieldwork. Biogeochemical analyses were performed with the invaluable assistance of B. Domeyer, M. Dibbern, R. Ebbinghaus, R. Suhrberg, S. Trinkler and V. Thoenissen. Preparation and deployment of large gears was smoothly achieved with the wizardry of S. Kriwanek, A. Petersen, M. Türk and S. Cherednichenko. We would also like to thank R. Schulz from the Laboratory for Radioisotopes (LARI) at the University of Göttingen for the ^{210}Pb analyses and helpful discussions with Volker Liebetrau. This work is a contribution of the Sonderforschungsbereich 754 "Climate–Biogeochemistry Interactions in the Tropical Ocean" (www.sfb754.de) which is supported by the Deutsche Forschungsgemeinschaft.

The service charges for this open access publication have been covered by a Research Centre of the Helmholtz Association.

References

Aller, R. C.: Bioturbation and remineralization of sedimentary organic matter: effects of redox oscillation, Chem. Geol., 114, 331–345, 1994.

Aller, R. C.: Mobile deltaic and continental shelf muds as suboxic, fluidized bed reactors, Mar. Chem., 61, 143–155, 1998.

Arnosti, C.: Speed bumps and barricades in the carbon cycle: substrate structural effects on carbon cycling, Mar. Chem., 92, 263–273, 2004.

BGD
11, 13067–13126, 2014

Arntz, W. E., Tarazona, J., Gallardo, V. A., Flores, L. A., and Salzwedel, H.: Benthos communities in oxygen deficient shelf and upper slope areas of the Peruvian and Chilean Pacific coast, and changes caused by El Niño, in: Modern and Ancient Continental Shelf Anoxia, edited by: Tyson, R. V. and Pearson, T. H., Geol. Soc. Spec. Publ., 58, 131–154, 1991.

Arthur, M. A., Dean, W. E., and Laarkamp, K.: Organic carbon accumulation and preservation in surface sediments on the Peru margin, Chem. Geol., 152, 273–286, 1998.

Ayón, P., Criales-Hernandez, M. I., Schwamborn, R., and Hirche, H. J.: Zooplankton research off Peru: a review, Prog. Oceanogr., 79, 238–255, 2008.

Berelson, W. M.: The flux of particulate organic carbon into the ocean interior: a comparison of four U.S. JGOFS regional studies, Oceanography, 14, 59–67, 2001.

Berelson, W. M., McManus, J., Coale, K. H., Johnson, K. S., Kilgore, T., Burdige, D., and Pilskaln, C.: Biogenic matter diagenesis on the sea floor: a comparison between two continental margin transects, J. Mar. Res., 54, 731–762, 1996.

Berner, R. A.: Burial of organic carbon and pyrite sulfur in the modern ocean; its geochemical and environmental significance, Am. J. Sci., 282, 451–473, 1982.

Berner, R. A.: The Phanerozoic Carbon Cycle: CO_2 and O_2, Oxford University Press, Oxford, 2004.

Bertrand, S., Díaz, E., and Lengaigne, M.: Patterns in the spatial distribution of Peruvian anchovy (*Engraulis ringens*) revealed by spatially explicit fishing data, Prog. Oceanogr., 79, 379–389, 2008.

Betts, J. N. and Holland, H. D.: The oxygen content of ocean bottom waters, the burial efficiency of organic carbon, and the regulation of atmospheric oxygen, Palaeogeogr. Palaeocl., 97, 5–18, 1991.

Bohlen, L., Dale, A. W., Sommer, S., Mosch, T., Hensen, C., Noffke, A., Scholz, F., and Wallmann, K.: Benthic nitrogen cycling traversing the Peruvian oxygen minimum zone, Geochim. Cosmochim. Ac., 75, 6094–6111, 2011.

Böning, P., Brumsack, H. J., Böttcher, M. E., Schnetger, B., Kriete, C., Kallmeyer, J., and Borchers, S. L.: Geochemistry of Peruvian near-surface sediments, Geochim. Cosmochim. Ac., 68, 4429–4451, 2004.

Bottjer, D. and Morales, C. E.: Nanoplanktonic assemblages in the upwelling area off Concepción (~ 36° S), central Chile: abundance, biomass, and grazing potential during the annual cycle, Prog. Oceanogr., 75, 415–434, 2007.

BGD
11, 13067–13126, 2014

Boudreau, B. P.: A method-of-lines code for carbon and nutrient diagenesis in aquatic sediments, Comput. Geosci., 22, 479–496, 1996.
Brandt, P., Banyte, D., Dengler, M., Didwischus, S.-H., Fischer, T., Greatbatch, R. J., Hahn, J., Kanzow, T., Karstensen, J., Körtzinger, A., Krahmann, G., Schmidtko, S., Stramma, L., Tanhua, T., and Visbeck, M.: On the role of circulation and mixing in the ventilation of oxygen minimum zones with a focus on the eastern tropical North Atlantic, Biogeosciences Discuss., 11, 12069–12136, doi:10.5194/bgd-11-12069-2014, 2014.
Burdige, D. J.: Sediment pore waters, in: Biogeochemistry of Marine Dissolved Organic Matter, edited by: Hansell, D. and Carlson, C., Academic Press, 611–663, 2002.
Burdige, D. J.: Geochemistry of Marine Sediments, Princeton University Press, Princeton, 2006.
Burdige, D. J.: Preservation of organic matter in marine sediments: controls, mechanisms, and an imbalance in sediment organic carbon budgets?, Chem. Rev., 107, 467–485, 2007.
Burwicz, E. B., Rüpke, L. H., and Wallmann, K.: Estimation of the global amount of submarine gas hydrates formed via microbial methane formation based on numerical reaction-transport modeling and a novel parameterization of Holocene sedimentation, Geochim. Cosmochim. Ac., 75, 4562–4576, 2011.
Calvert, S. E., Bustin, R. M., and Pedersen, T. F.: Lack of evidence for enhanced preservation of sedimentary organic matter in the oxygen minimum of the Gulf of California, Geology, 20, 757–760, 1992.
Canfield, D. E.: Organic matter oxidation in marine sediments, in: Interactions of C, N, P and S Biogeochemical Cycles and Global Change, edited by: Wollast, R., Mackenzie, F. T., and Chou, L., NATO ASI Ser. I, 4, 333–364, Springer, Berlin, 1993.
Canfield, D. E.: Factors influencing organic carbon preservation in marine sediments, Chem. Geol., 114, 315–329, 1994.
CARS: CSIRO Atlas of Regional Seas, available at: http://www.marine.csiro.au/~dunn/cars2009 (last access: 12 August 2014), 2014.
Carton, J. A. and Giese, B. S.: A reanalysis of ocean climate using Simple Ocean Data Assimilation (SODA), Mon. Weather Rev., 136, 2999–3017, 2008.
Coppola, L., Gustafsson, O., Andersson, P., Eglinton, T. I., Uchida, M., and Dickens, A. F.: The importance of ultrafine particles as a control on the distribution of organic carbon in Washington Margin and Cascadia Basin sediments, Chem. Geol., 243, 142–156, 2007.

BGD
11, 13067–13126, 2014

Cowie, G. L. and Hedges, J. H.: Biochemical indicators of diagenetic alteration in natural organic matter mixtures, Nature, 369, 304–307, 1994.

Da Silva, A. M., Young, C. C., and Levitus, S.: Atlas of Surface Marine Data 1994, vol. 1, Algorithms and Procedures, technical report, Natl. Oceanogr. Atmos. Admin., Silver Spring, MD, 1994.

Dale, A. W., Bertics, V. J., Treude, T., Sommer, S., and Wallmann, K.: Modeling benthic–pelagic nutrient exchange processes and porewater distributions in a seasonally hypoxic sediment: evidence for massive phosphate release by *Beggiatoa*?, Biogeosciences, 10, 629–651, doi:10.5194/bg-10-629-2013, 2013.

Dale, A. W., Sommer, S., Ryabenko, E., Noffke, A., Bohlen, L., Wallmann, K., Stolpovsky, K., Greinert, J., and Pfannkuche, O.: Benthic nitrogen fluxes and fractionation of nitrate in the Mauritanian oxygen minimum zone (Eastern Tropical North Atlantic), Geochim. Cosmochim. Ac., 134, 234–256, 2014.

Dauwe, B., Middelburg, J. J., Herman, P. M. J., and Heip, C. H. R.: Linking diagenetic alteration of amino acids and bulk organic matter reactivity, Limnol. Oceanogr., 44, 1809–1814, 1999.

Demaison, G. J. and Moore, G. T.: Anoxic environments and oil source bed genesis, Am. Assoc. Petr. Geol. B., 64, 1179–1209, 1980.

Devol, A. H. and Hartnett, H. E.: Role of the oxygen-deficient zone in transfer of organic carbon to the deep ocean, Limnol. Oceanogr., 46, 1684–1690, 2001.

Dunne, J. P., Sarmiento, J. L., and Gnanadesikan, A.: A synthesis of global particle export from the surface ocean and cycling through the ocean interior and on the seafloor, Global Biogeochem. Cy., 21, GB4006, doi:10.1029/2006GB002907, 2007.

Echevin, V., Aumont, O., Ledesms, J., and Flores, G.: The seasonal cycle of surface chlorophyll in the Peruvian upwelling system: a modelling study, Prog. Oceanogr., 79, 167–176, 2008.

Fiedler, P. C. and Talley, L. D.: Hydrography of the eastern tropical Pacific: a review, Prog. Oceanogr., 69, 143–180, 2006.

Flögel, S., Wallmann, K., Poulsen, C. J., Zhou, J., Oschlies, A., Voigt, S., and Kuhnt, W.: Simulating the biogeochemical effects of volcanic CO_2 degassing on the oxygen-state of the deep ocean during the Cenomanian/Turonian Anoxic Event (OAE2), Earth Planet. Sc. Lett., 305, 371–384, 2011.

Fuenzalida, R., Schneider, W., Garcés-Vargas, J., Bravo, L., and Lange, C.: Vertical and horizontal extension of the oxygen minimum zone in the eastern South Pacific Ocean, Deep-Sea Res.Pt. II, 56, 1027–1038, 2009.

BGD
11, 13067–13126, 2014

Gagosian, R. B., Nigrelli, G. E., and Volkman, J. K.: Vertical transport and transformation of biogenic organic compounds from a sediment trap experiment off the coast of Peru, in: Coastal Upwelling, its Sediment Record. Part A, edited by: Suess, E. and Thiede, J., Plenum Press, New York, 241–272, 1983.

Gallardo, V. A.: Large benthic microbial communities in sulphide biota under Peru–Chile subsurface countercurrent, Nature, 268, 331–332, 1977.

Giering, S. L. C., Sanders, R., Lampitt, R. S., Anderson, T. R., Tamburini, C., Boutrif, M., Zubkov, M. V., Marsay, C. M., Henson, S. A., Saw, K., Cook, K., and Mayor, D. J.: Reconciliation of the carbon budget in the ocean's twilight zone, Nature, 507, 480–483, 2014.

Glenn, C. R. and Arthur, M. A.: Petrology and major element geochemistry of Peru margin phosphorites and associated diagenetic minerals: authigenesis in modern organic-rich sediments, Mar. Geol., 80, 231–267, 1988.

Grasshoff, K., Ehrhardt, M., and Kremling, K.: Methods of Seawater Analysis, Wiley-VCH, Weinheim, 1999.

Gutiérrez, D., Gallardo, V. A., Mayor, S., Neira, C., Vásquez, C., Sellanes, J., Rivas, M., Soto, A., Carrasco, F., and Baltaza, M.: Effects of dissolved oxygen and fresh organic matter on the bioturbation potential of macrofauna in sublittoral sediments off Central Chile during the 1997/1998 El Niño, Mar. Ecol.-Prog. Ser., 202, 81–99, 2000.

Gutiérrez, D., Enríquez, E., Purca, S., Quipúzcoa, L., Marquina, R., Flores, G., and Graco, M.: Oxygenation episodes on the continental shelf of central Peru: remote forcing and benthic ecosystem response, Prog. Oceanogr., 79, 177–189, 2008.

Gutiérrez, D., Sifeddine, A., Field, D. B., Ortlieb, L., Vargas, G., Chávez, F. P., Velazco, F., Ferreira, V., Tapia, P., Salvatteci, R., Boucher, H., Morales, M. C., Valdés, J., Reyss, J.-L., Campusano, A., Boussafir, M., Mandeng-Yogo, M., García, M., and Baumgartner, T.: Rapid reorganization in ocean biogeochemistry off Peru towards the end of the Little Ice Age, Biogeosciences, 6, 835–848, doi:10.5194/bg-6-835-2009, 2009.

Gutknecht, E., Dadou, I., Marchesiello, P., Cambon, G., Le Vu, B., Sudre, J., Garçon, V., Machu, E., Rixen, T., Kock, A., Flohr, A., Paulmier, A., and Lavik, G.: Nitrogen transfers off Walvis Bay: a 3-D coupled physical/biogeochemical modeling approach in the Namibian upwelling system, Biogeosciences, 10, 4117–4135, doi:10.5194/bg-10-4117-2013, 2013.

Haake, B., Ittekkot, V., Ramaswamy, V., Nairb, R. R., and Honjo, S.: Fluxes of amino acids and hexosamines to the deep Arabian Sea, Mar. Chem., 40, 291–314, 1992.

BGD
11, 13067–13126, 2014

Haffert, L., Haeckel, M., Liebetrau, V., Berndt, C., Hensen, C., Nuzzo, M., Reitz, A., Scholz, F., Schönfeld, J., Perez-Garcia, C., and Weise, S. M.: Fluid evolution and authigenic mineral paragenesis related to salt diapirism – the Mercator mud volcano in the Gulf of Cadiz, Geochim. Cosmochim. Ac., 106, 261–286, 2013.

Hedges, J. I. and Keil, R. G.: Sedimentary organic matter preservation: an assessment and speculative synthesis, Mar. Chem., 49, 81–115, 1995.

Hedges, J. I., Hu, F. S., Devol, A. H., Hartnett, H. E., Tsamakis, E., and Keil, R. G.: Sedimentary organic matter preservation: a test for selective degradation under oxic conditions, Am. J. Sci., 299, 529–555, 1999.

Henrichs, S. M. and Farrington, J. W.: Peru upwelling region sediments near 15° S. 1. Remineralization and accumulation of organic matter, Limnol. Oceanogr., 29, 1–19, 1984.

Henrichs, S. M. and Reeburgh, W. S.: Anaerobic mineralization of marine sediment organic matter: rates and the role of anaerobic processes in the oceanic carbon economy, Geomicrobiol. J., 5, 191–237, 1987.

Hinga, K. R., Sieburth, J., and Heath, G. R.: The supply and use of organic material at the deep – sea floor, J. Mar. Res., 37, 557–579, 1979.

Huettel, M., Forster, S., Kloser, S., and Fossing, H.: Vertical migration in the sediment-dwelling sulfur bacteria *Thioploca* spp. in overcoming diffusion limitations, Appl. Environ. Microb., 62, 1863–1872, 1996.

Hulthe, G., Hulth, S., and Hall, P. O. J.: Effect of oxygen on degradation rate of refractory and labile organic matter in continental margin sediments, Geochim. Cosmochim. Ac., 62, 1319–1328, 1998.

Hunter, W. R., Veuger, B., and Witte, U.: Macrofauna regulate heterotrophic bacterial carbon and nitrogen incorporation in low-oxygen sediments, ISME J., 6, 2140–2151, 2012.

Jahnke, R. A., Reimers, C. E., and Craven, D. B.: Intensification of recycling of organic matter at the sea floor near ocean margins, Nature, 348, 50–54, 1990.

Jordán, R. S.: Distribution of anchoveta (*Engraulis ringens* J.) in relation to the environment, Investigaciones Pesquera, 35, 113–126, 1971.

Jørgensen, B. B. and Gallardo, V. A.: *Thioploca* spp: filamentous sulfur bacteria with nitrate vacuoles, FEMS Microbiol. Ecol., 28, 301–313, 1999.

Kalvelage, T., Lavik, G., Lam, P., Contreras, S., Arteaga, L., Löscher, C. R., Oschlies, A., Paulmier, A., Stramma, L., and Kuypers, M. M. M.: Nitrogen cycling driven by organic matter export in the South Pacific oxygen minimum zone, Nat. Geosci., 6, 228–234, 2013.

BGD
11, 13067–13126, 2014

Keil, R. G. and Cowie, G. L.: Organic matter preservation through the oxygen-deficient zone of the NE Arabian Sea as discerned by organic carbon: mineral surface area ratios, Mar. Geol., 161, 13–22, 1999.
Keil, R. G., Montlucon, D. B., Prahl, F. G., and Hedges, J. I.: Sorptive preservation of labile organic matter in marine sediments, Nature, 370, 549–552, 1994.
Kim, K. H. and Burnett, W. C.: Accumulation and biological mixing of Peru margin sediments, Mar. Geol., 80, 181–194, 1988.
Koho, K. A., Nierop, K. G. J., Moodley, L., Middelburg, J. J., Pozzato, L., Soetaert, K., van der Plicht, J., and Reichart, G-J.: Microbial bioavailability regulates organic matter preservation in marine sediments, Biogeosciences, 10, 1131–1141, doi:10.5194/bg-10-1131-2013, 2013.
Koné, V., Machu, E., Penven, P., Andersen, V., Garçon, V., Fréon, P., and Demarcq, H.: Modeling the primary and secondary productions of the southern Benguela upwelling system: a comparative study through two biogeochemical models, Global Biogeochem. Cy., 19, GB4021, 2005.
Kriest, I. and Oschlies, A.: Swept under the carpet: organic matter burial decreases global ocean biogeochemical model sensitivity to remineralization length scale, Biogeosciences, 10, 8401–8422, doi:10.5194/bg-10-8401-2013, 2013.
Krissek, L. A., Scheideddger, K. F., and Kulm, L. V.: Surface sediments of the Peru–Chile continental margin and the Nazca plate, Geol. Soc. Am. Bull., 91, 321–331, 1980.
Lam, P., Lavik, K., Jensen, M. M., van de Vossenberg, J., Schmid, M., Woebken, D., Gutiérrez, D., Amann, R., Jetten, M. S. M., and Kuypers, M. M. M.: Revising the nitrogen cycle in the Peruvian oxygen minimum zone, P. Natl. Acad. Sci. USA, 106, 4752–4757, 2009.
Lasaga, A. C. and Holland, H. D.: Mathematical aspects of non-steady-state diagenesis, Geochim. Cosmochim. Ac., 40, 257–266, 1976.
Levin, L., Gutiérrez, D., Rathburn, A., Neira, C., Sellanes, J., Muñoz, P., Gallardo, V., and Salamanca, M.: Benthic processes on the Peru margin: a transect across the oxygen minimum zone during the 1997–98 El Niño, Prog. Oceanogr., 53, 1–27, 2002.
Levipan, H. A., Quińones, R. A., and Urrutia, H.: A time series of prokaryote secondary production in the oxygen minimum zone of the Humboldt current system, off central Chile, Prog. Oceanogr., 75, 531–545, 2007.

BGD
11, 13067–13126, 2014

Lomstein, B. A., Niggemann, J., Jørgensen, B. B., and Langerhuus, A. T.: Accumulation of prokaryotic remains during organic matter diagenesis in surface sediments off Peru, Limnol. Oceanogr., 54, 1139–1151, 2009.
Liu, W. T., Tang, W., and Polito, P. S.: NASA scatterometer provides global ocean-surface wind fields with more structures than numerical weather prediction, Geophys. Res. Lett., 25, 761–764, 1998.
Martin, J. H., Knauer, G. A., Karl, D. M., and Broenkow, W. W.: VERTEX: carbon cycling in the northeast Pacific, Deep-Sea Res., 34, 267–285, 1987.
Mayer, L. M.: Surface area control of organic carbon accumulation in continental shelf sediments, Geochim. Cosmochim. Ac., 58, 1271–1284, 1994.
Meile, C. and Van Cappellen, P.: Particle age distributions and O_2 exposure times: timescales in bioturbated sediments, Global Biogeochem. Cy., 19, GB3013, doi:10.1029/2004GB002371, 2005.
Montes, I., Dewitte, B., Gutknecht, E., Paulmier, A., Dadou, I., Oschlies, A., and Garçon, V.: High-resolution modeling of the Eastern Tropical Pacific Oxygen Minimum Zone: sensitivity to the tropical oceanic circulation, J. Geophys. Res., submitted, 2014.
Moodley, L., Nigam, R., Ingole, B., Prakash Babu, C., Panchang, R., Nanajkar, M., Sivadas, S., van Breugel, P., van Ijzerloo, L., Rutgersa, R., Heip, C. H. R., Soetaert, K., and Middelburg, J. J.: Oxygen minimum seafloor ecological (mal) functioning, J. Exp. Mar. Biol. Ecol., 398, 91–100, 2011.
Morales, C. E., Hormazabal, S. E., and Blanco, J. L.: Interannual variability in the mesoscale distribution of the depth of the upper boundary of the oxygen minimum layer off northern Chile (18–24° S): implications for the pelagic system and biogeochemical cycling, J. Mar. Res., 57, 909–932, 1999.
Morel, A. and Berthon, J. A.: Surface pigments, algal biomass profiles, and potential production of the euphotic layer: relationships reinvestigated in view of remote-sensing applications, Limnol. Oceanogr., 34, 1545–1562, 1989.
Mosch, T., Sommer, S., Dengler, M., Noffke, A., Bohlen, L., Pfannkuche, O., Liebetrau, V., and Wallmann, K.: Factors influencing the distribution of epibenthic megafauna across the Peruvian oxygen minimum zone, Deep-Sea Res. Pt. I, 68, 123–135, 2012.
Müller, P. J. and Suess, E.: Productivity, sedimentation rate, and sedimentary organic matter in the oceans – I. Organic carbon preservation, Deep-Sea Res., 26, 1347–1362, 1979.

BGD
11, 13067–13126, 2014

Niggemann, J. and Schubert, C. J.: Sources and fate of amino sugars in coastal Peruvian sediments, Geochim. Cosmochim. Ac., 70, 2229–2237, 2006.
Noffke, A., Hensen, C., Sommer, S., Scholz, F., Bohlen, L., Mosch, T., Graco, M., and Wallmann, K.: Benthic iron and phosphorus fluxes across the Peruvian oxygen minimum zone, Limnol. Oceanogr., 57, 851–867, 2012.
O'Reilly, J. E., Maritorena, S., Siegel, D. A., O'Brien, M. C., Toole, D., Chavez, F. P., Strutton, P., Cota, G. F., Hooker, S. B., McClain, C. R., Carder, K. L., Muller-Karger, F., Harding, L., Magnuson, A., Phinney, D., Moore, G. F., Aiken, J., Arrigo, K. R., Letelier, R., and Culver, M.: Ocean chlorophyll *a* algorithms for SeaWiFS, OC2, and OC4: Version 4, in: SeaWiFS Post Launch Calibration and Validation Analyses, Part 3, edited by: O'Reilly, J. E., NASA Technical Memorandum 2000-206892, 11, 9–19, 2000.
Otsuki, A. and Hanja, T.: Production of dissolved organic matter from dead green algal cells. II. Anaerobic microbial decomposition, Limnol. Oceanogr., 17, 258–264, 1972.
Parkes, R. J., Cragg, B. A., Getlifff, J. M., Harvey, S. M., Fry, J. C., Lewis, C. A., and Rowland, S. J.: A quantitative study of microbial decomposition of biopolymers in Recent sediments from the Peru Margin, Mar. Geol., 113, 55–66, 1993.
Pedersen, T. F. and Calvert, S. E.: Anoxia vs. productivity: what controls the formation of organic carbon-rich sediments and sedimentary rocks?, Am. Assoc. Petr. Geol. B., 74, 454–466, 1990.
Pennington, J. T., Mahoney, K. L., Kuwahara, V. S., Kolber, D. D., Calienes, R., and Chavez, F. P.: Primary production in the eastern tropical Pacific: a review, Prog. Oceanogr., 69, 285–317, 2006.
Quiñones, R. A., Gutierrez, M. H., Daneri, G., Aguilar, D. G., Gonzalez, H. E., and Chavez, F. P.: The Humboldt Current System, in: Carbon and Nutrient Fluxes in Continental Margins: a Global Synthesis, edited by: Liu, K.-K., Atkinson, L., Quiñones, R., and Talaue-McManus, L., Springer-Verlag, Berlin, 44–64, 2010.
Redfield, A. C., Ketchum, B. H., and Richards, F. A.: The influence of organisms on the composition of seawater, in: The Sea, edited by: Hill, M. N., Interscience, New York, 26–77, 1963
Reimers, C. E. and Suess, E.: The partitioning of organic carbon fluxes and sedimentary organic matter decomposition rates in the ocean, Mar. Chem., 13, 141–168, 1983a.
Reimers, C. E. and Suess, E.: Late Quaternary fluctuations in the cycling of organic matter off central Peru: a proto-kerogen record, in: Coastal Upwelling, its Sediment Record. Part A, edited by: Suess, E. and Thiede, J., Plenum Press, New York, 497–526, 1983b.

BGD
11, 13067–13126, 2014

Reimers, C. E. and Suess, E.: Spatial and temporal patterns of organic matter accumulation on the Peru continental margin, in: Coastal Upwelling, its Sediment Record. Part B, edited by: Suess, E. and Thiede, J., Plenum Press, New York, 311–345, 1983c.
Reimers, C. E., Jahnke, R. A., and McCorkle, D. C.: Carbon fluxes and burial rates over the continental slope and rise off central California with implications for the global carbon cycle, Global Biogeochem. Cy., 6, 199–224, 1992.
Ryan, J. P., Ueki, I., Chao, Y., Zhang, H., Polito, P. S., and Chavez, F. P.: Western Pacific modulation of large phytoplankton blooms in the central and eastern equatorial Pacific, J. Geophys. Res., 111, G02013, doi:10.1029/2005JG000084, 2006.
Sarmiento, J. L. and Gruber, N.: Ocean Biogeochemical Dynamics, Princeton University Press, Princeton, 2006.
Schlanger, S. O. and Jenkyns, H. C.: Cretaceous oceanic anoxic events: causes and consequences, Geol. Mijnbouw, 55, 179–184, 1976.
Schönfeld, J., Kuhnt, W., Erdem, Z., Flögel, S., Glock, N., Aquit, M., Frank, M., and Holbourn, A.: Systematics of past changes in ocean ventilation: a comparison of Cretaceous Ocean Anoxic Event 2 and Pleistocene to Holocene Oxygen Minimum Zones, Biogeosciences Discuss., submitted, 2014.
Shchepetkin, A. F. and McWilliams, J. C.: A method for computing horizontal pressure-gradient force in an oceanic model with a nonaligned vertical coordinate, J. Geophys. Res., 108, C3, 3090, doi:10.1029/2001JC001047, 2003.
Scholz, F., Hensen, C., Noffke, A., Rohde, A., Liebetrau, V., and Wallmann, K.: Early diagenesis of redox-sensitive trace metals in the Peru upwelling area – response to ENSO-related oxygen fluctuations in the water column, Geochim. Cosmochim. Ac., 75, 7257–7276, 2011.
Seiter, K., Hensen, C., Schröter, J., and Zabel, M.: Organic carbon content in surface sediments – defining regional provinces, Deep-Sea Res.Pt. I, 51, 2001–2026, 2004.
Sommer, S., Türk, M., Kriwanek, S., and Pfannkuche, O.: Gas exchange system for extended in situ benthic chamber flux measurements under controlled oxygen conditions: first application – sea bed methane emission measurements at Captain Arutyunov mud volcano, Limnol. Oceanogr.-Meth., 6, 23–33, 2008.
Staresinic, N., Farrington, J., and Gagosian, R. B.: Downward transport of particulate matter in the PEru coastal upwelling: role of the anchoveta, in: Coastal Upwelling, its Sediment Record. Part A, edited by: Suess, E. and Thiede, J., Plenum Press, New York, 225–240, 1983.

BGD
11, 13067–13126, 2014

Stramma, L., Bange, H. W., Czeschel, R., Lorenzo, A., and Frank, M.: On the role of mesoscale eddies for the biological productivity and biogeochemistry in the eastern tropical Pacific Ocean off Peru, Biogeosciences, 10, 7293–7306, doi:10.5194/bg-10-7293-2013, 2013.
Suess, E.: Particulate organic carbon flux in the oceans – surface productivity and oxygen utilization, Nature, 288, 260–263, 1980.
Suess, E.: Phosphate regeneration from sediments of the Peru continental margin by dissolution of fish debris, Geochim. Cosmochim. Ac., 45, 577–588, 1981.
Suess, E., Kulm, L. D., and Killingley, J. S.: Coastal upwelling and a history of organic-rich mudstone deposition off Peru, in: Marine Petroleum Source Rocks, edited by: Brooks, J. and Fleet, A. J., Geol. Soc. Spec. Publ., 26, 181–197, 1987.
Suntharalingam, P., Sarmiento, J. L., and Toggweiler, J. R.: Global significance of nitrous-oxide production and transport from oceanic low-oxygen zones: a modeling study, Global Biogeochem. Cy., 14, 1353–1370, 2000.
Suntharalingam, P., Buitenhuis, E., Le Quere, C., Dentener, F., Nevinson, C., Butler, L., Bange, H., and Forster, G.: Quantifying the impact of anthropogenic nitrogen deposition on oceanic nitrous oxide, Geophys. Res. Lett., 39, L07605, 2012.
Tam, J., Taylor, M. H., Blaskovic, V., Espinoza, P., Ballón, R. M., Díaz, E., Wosnitza-Mendo, C., Argüelles, J., Purca, S., Ayón, P., Quipuzcoa, L., Gutiérrez, D., Goya, E., Ochoa, N., and Wolff, M.: Trophic modeling of the Northern Humboldt Current ecosystem, Part I: Comparing trophic linkages under La Niña and El Niño conditions, Prog. Oceanogr., 79, 352–365, 2008.
Tarazona, J., Salzwedel, H., and Arntz, W.: Positive effects of "El Niño" on macrozoobenthos inhabiting hypoxic areas of the Peruvian upwelling system, Oecologia, 76, 184–190, 1988.
Turnewitsch, R., Witte, U., and Graf, G.: Bioturbation in the abyssal Arabian Sea: influence of fauna and food supply, Deep-Sea Res. Pt. II, 47, 2877–2911, 2000.
Van Mooy, B. A. S., Keil, R. G., and Devol, A. H.: Impact of suboxia on sinking particulate organic carbon: enhanced carbon flux and preferential degradation of amino acids via denitrification, Geochim. Cosmochim. Ac., 66, 457–465, 2002.
Vandewiele, S., Cowie, G., Soetaert, K., and Middelburg, J. J.: Amino acid biogeochemistry and organic matter degradation state across the Pakistan margin oxygen minimum zone, Deep-Sea Res. Pt. II, 56, 318–334, 2009.
Wallmann, K. and Aloisi, G.: The Global Carbon Cycle: geological processes, in: Fundamentals of Geobiology, edited by: Knoll, A. H., Canfield, D. E., and Konhauser., K. O., Blackwell Publishing Ltd., 20–35, 2012.

BGD
11, 13067–13126, 2014

Walsh, J. J.: A carbon budget for overfishing off Peru, Nature, 290, 300–304, 1981.
Westrich, J. T. and Berner, R. A.: The role of sedimentary organic matter in bacterial sulfate reduction: the G-model tested, Limnol. Oceanogr., 29, 236–249, 1984.
Witte, U., Wenzhöfer, F., Sommer, S., Boetius, A., Heinz, P., Aberle, N., Sand, M., Cremer, A., Abraham, W.-R., Jørgensen, B. B., and Pfannkuche, O.: In situ experimental evidence of the fate of a phytodetritus pulse at the abyssal sea floor, Nature, 424, 763–766, 2003.
Wolf-Gladrow, D. A., Zeebe, R. E., Klaas, C., Körtzinger, A., and Dickson, A. G.: Total alkalinity: the explicit conservative expression and its application to biogeochemical processes, Mar. Chem., 106, 287–300, 2007.
Yakusev, E. V., Pollehne, F., Jost, G., Kuznetso, I., Schneider, B., and Urnlauf, L.: Analysis of the water column oxic/anoxic interface in the Black and Baltic seas with a numerical model, Mar. Chem., 107, 388–410, 2000.
Yu, E. F., Francois, R., Bacon, M. P., Honjo, S., Fleer, A. P., Manganini, S. J., Rutgers van der Loeff, M. M., Ittekot, V.: Trapping efficiency of bottom-tethered sediment traps estimated from the intercepted fluxes of ^{230}Th and ^{231}Pa, Deep-Sea Res. Pt. I, 48, 865–889, 2001.
Zeebe, R. E. and Wolf-Gladrow, D. A.: CO_2 in Seawater: Equilibrium, Kinetics, Isotopes, Elsevier Oceanography Series, Amsterdam, 2001.
Zonneveld, K. A. F., Versteegh, G. J. M., Kasten, S., Eglinton, T. I., Emeis, K.-C., Huguet, C., Koch, B. P., de Lange, G. J., de Leeuw, J. W., Middelburg, J. J., Mollenhauer, G., Prahl, F. G., Rethemeyer, J., and Wakeham, S. G.: Selective preservation of organic matter in marine environments; processes and impact on the sedimentary record, Biogeosciences, 7, 483–511, doi:10.5194/bg-7-483-2010, 2010.

BGD
11, 13067–13126, 2014

Table 1. Stations and gears deployed on the Peruvian margin. Water depths were recorded from the ship's winch and bottom water temperature and dissolved oxygen were measured using a CTD.

Station	Gear[a]	Date	Latitude (S)	Longitude (W)	Depth (m)	Temp. (°C)	O_2[b] (°C)
	11° S						
1	BIGO 5	15 Nov 2008	11°00.02′	77°47.72′	85	12.7	bdl
	MUC 52	12 Nov 2008	10°59.99′	77°47.40′	78		
2	BIGO-T6[c]	29 Nov 2008	10°59.80′	78°05.91′	259	12.2	bdl
3	BIGO 1	05 Nov 2008	11°00.00′	78°09.92′	315	11.6	bdl
	MUC 19	03 Nov 2008	11°00.01′	78°09.97′	319		
4	BIGO 3	20 Nov 2008	11°00.02′	78°15.27′	397	9.6	bdl
	MUC 33	06 Nov 2008	11°00.00′	78°14.19′	376		
5	BIGO 2	05 Nov 2008	11°00.01′	78°25.55′	695	6.7	6.2
	MUC 25	04 Nov 2008	11°00.03′	78°25.60′	697		
6	BIGO 6[c]	29 Nov 2008	10°59.82′	78°31.05′	978	4.7	40.3
	MUC 53	13 Nov 2008	10°59.81′	78°31.27′	1005		
	12° S						
1	BIGO I–II	15 Jan 2013	12°13.506′	77°10.793′	74	14.0	bdl
	MUC 13	11 Jan 2013	12°13.496′	77°10.514′	71		
	MUC 39	25 Jan 2013	12°13.531′	77°10.061′	72		
2	BIGO I–V	27 Jan 2013	12°14.898′	77°12.705′	101	13.8	bdl
	MUC 16	12 Jan 2013	12°14.897′	77°12.707′	103		
3	BIGO II–IV	20 Jan 2013	12°16.689′	77°14.995′	128	13.7	bdl
	MUC 46	27 Jan 2013	12°16.697′	77°15.001′	129		
4	BIGO I–I	11 Jan 2013	12°18.711′	77°17.803′	142	13.4	bdl
	MUC 10	09 Jan 2013	12°18.708′	77°17.794′	145		
5	BIGO I–IV	23 Jan 2013	12°21.502′	77°21.712′	195	13.0	bdl
	MUC 45	27 Jan 2013	12°21.491′	77°21.702′	195		
6	BIGO II–II	12 Jan 2013	12°23.301′	77°24.284′	244	12.0	bdl
	MUC 5	07 Jan 2013	12°23.329′	77°24.185′	253		
	MUC 34	23 Jan 2013	12°23.300′	77°24.228′	244		
7	BIGO II–I	08 Jan 2013	12°24.905′	77°26.295′	306	12.5	bdl
	MUC 9	08 Jan 2013	12°24.894′	77°26.301′	304		
	MUC 36	24 Jan 2013	12°25.590′	77°25.200′	297		
8	BIGO II–V	24 Jan 2013	12°27.207′	77°29.517′	409	10.6	bdl
	MUC 23	15 Jan 2013	12°27.198′	77°29.497′	407		
	MUC 24	15 Jan 2013	12°27.195′	77°29.483′	407		
9	BIGO II–III	16 Jan 2013	12°31.366′	77°34.997′	756	5.5	19
	MUC 17	13 Jan 2013	12°31.374′	77°35.183′	770		
10	BIGO I–III	19 Jan 2013	12°34.911′	77°40.365′	989	4.4	53
	MUC 28	19 Jan 2013	12°35.377′	77°40.975′	1024		

[a] The first Roman numeral of the BIGO code for 12° S denotes the lander used and the second to the deployment number of that lander. For 11° S, the Arabic number refers to the deployment number. The lander at St. 2 is denoted BIGO-T as described in the text.
[b] bdl = below detection limit (5 µM).
[c] These deployments occurred during leg 2 of cruise M77. All others from 11° S took place during leg 1.

BGD
11, 13067–13126, 2014

Table 2. Measured and modeled particulate organic carbon rain rates, accumulation rates, and burial efficiencies.

	Inner shelf		Outer shelf			OMZ			Below OMZ	
12° S transect	St. 1	St. 2	St. 3	St. 4	St. 5	St. 6	St. 7	St. 8	St. 9	St. 10
Measured data										
Water depth, m	74	101	128	142	195	244	306	409	756	989
Sediment accumulation rate (ω_{acc}), cm yr^{-1} [a]	0.45	0.32	0.2	0.04	0.1	0.07	0.05	0.011	0.035	0.06
Mass accumulation rate (MAR), g m^{-2} yr^{-1} [b]	1800	768	600	128	320	182	150	44	259	540
POC content at 10 cm (POC$_{10}$),% [c]	3.3	3.8	7.2	8.6	12.8	14.2	15.5	5.2	4.0	1.8
POC accumulation rate at 10 cm (POC$_{AR10}$), g C m^{-2} yr^{-1} [d]	60	29	34	11	41	26	23	2	10	10
Benthic DIC flux (J_{DIC}), mmol m^{-2} d^{-1} [e]	65.9 ± 21	27.9 ± 4.2	20.4 ± 7	8.0 ± 0.4	3.2 ± 1	4.7 ± 1	2.7 ± 0.1	2.2 ± 0.3	2.8 ± 3	1.2 ± 0.1
POC rain rate (RRPOC), mmol m^{-2} d^{-1} [f]	79.5 ± 33	34.2 ± 11	28.2 ± 12	10.5 ± 3	12.5 ± 6	10.6 ± 4	8.0 ± 2	2.7 ± 1	5.2 ± 5	3.4 ± 1
Carbon burial efficiency at 10 cm (CBE), % [g]	17 ± 7	19 ± 6	28 ± 12	24 ± 7	74 ± 37	55 ± 23	66 ± 19	19 ± 6	46 ± 48	64 ± 19
Modeled data										
POC accumulation rate at 10 cm, g C m^{-2} yr^{-1} [h]	59	29	34	9	38	27	26	2	11	12
Benthic DIC flux, mmol m^{-2} d^{-1}	61.8	27.9	18.0	8.4	5.2	4.9	4.0	2.2	3.3	1.7
POC rain rate, mmol m^{-2} d^{-1} [j]	75.3	34.5	25.9	10.6	13.9	11.1	10.0	2.6	5.8	4.4
Carbon burial efficiency at 10 cm, % [k]	18	19	30	20	62	56	60	15	43	61
11° S transect	St. 1					St. 2	St. 3	St. 4	St. 5	St. 6
Measured data										
Water depth, m	85					259	315	397	695	978
Sediment accumulation rate (ω_{acc}), cm yr^{-1} [m]	0.3					0.06	0.05	0.05	0.08	0.052
Mass accumulation rate (MAR), g m^{-2} yr^{-1} [b]	1200					132	150	370	464	343
POC content at 10 cm (POC$_{10}$), % [n]	2.4					14.2	15.3	12.6	6.8	3.8
POC accumulation rate at 10 cm (POC$_{AR10}$), g C m^{-2} yr^{-1} [d]	29					19	23	46	32	13
Modeled data										
POC accumulation rate at 10 cm, g C m^{-2} yr^{-1} [h]	31					16	17	44	32	16
Benthic DIC flux, mmol m^{-2} d^{-1} [p]	8.2					7.7	5.9	4.0	1.7	2.1
POC rain rate, mmol m^{-2} d^{-1} [j]	15.3					11.4	9.8	14.0	9.0	5.9
Carbon burial efficiency at 10 cm, % [k]	47					32	40	71	81	64

[a] Determined from $^{210}Pb_{xs}$ (see Table S2 in the Supplement). Sedimentation rates at St. 2 (101 m) and St. 6 (250 m) were not measured and instead estimated from the neighboring stations. ω_{acc} has a 20 % uncertainty.
[b] Calculated as $\omega_{acc} \times (1 - \varphi\,(L)) \times \rho \times 10\,000$ (ρ = dry solid density, 2 g cm^{-3}).
[c] For St. 8 at 12° S (409 m) the content at 3 cm was taken since the underlying sediment is old, non-accumulating clay. For the OMZ stations the mean POC content in the upper 10 cm was used instead. This was approximated as follows: $POC_{10}\ (\%) = \frac{1}{10}\int_0^{10} POC(x)\,dx$ where $POC(x)$ is in %.
[d] Calculated as MAR × POC$_{10}$/100.
[e] Mean fluxes calculated from the in situ TA and pCO_2 measurements in two benthic chambers. No pCO_2 measurements were made at 11° S. Errors represent 50 % of the difference of the two fluxes.
[f] Calculated as POC$_{AR10}$ (in mmol m^{-2} d^{-1}) + J_{DIC}.
[g] Calculated as POC$_{AR10}$ (in mmol m^{-2} d^{-1})/RRPOC × 100 %. Errors were calculated using standard error propagation rules assuming a 20 % uncertainty in ω_{acc} and POC$_{10}$.
[h] Calculated analogously to footnote [d] using modeled data.
[j] Calculated analogously to footnote [f] using modeled data.
[k] Calculated analogously to footnote [g] using modeled data.
[m] Determined from $^{210}Pb_{xs}$ modeling (see Bohlen et al., 2011).
[n] For the OMZ stations, the mean POC content in the upper 10 cm was used (see footnote c).
[p] Calculated as the depth-integrated POC degradation rate (Bohlen et al., 2011).

BGD
11, 13067–13126, 2014

Table 3. Mean rates of organic carbon accumulation on the Peruvian margin from this study compared to global averages by Burdige (2007) and Sarmiento and Gruber (2006) (units: mmol m^{-2} d^{-1}).

	11° S	12° S	Burdige (2007)[a]	Sarmiento and Gruber (2006)[b]
Shelf (0–200 m)	13.8	9.9	4.0	–
Upper slope (200–1000 m)	7.2	2.8	1.0	–
Total margin (0–1000 m)	6.8	6.1	2.9 (2.0)	1.4
Deep sea (> 1000 m)	–	–	0.062	0.013

[a] From Table 4 and 5 in Burdige (2007) based on a large number of independent studies. The number in parenthesis is the total rate considering low POC burial rates in sandy sediments.
[b] From Table 6.5.1 in that study, derived largely from earlier studies by Berner (1982) and Wollast (1993). Note that their area of the margin < 1000 m (2.76×10^{13} m^2) is 36 % lower than that used by Burdige (2007) (4.31×10^{13} m^2).

BGD
11, 13067–13126, 2014

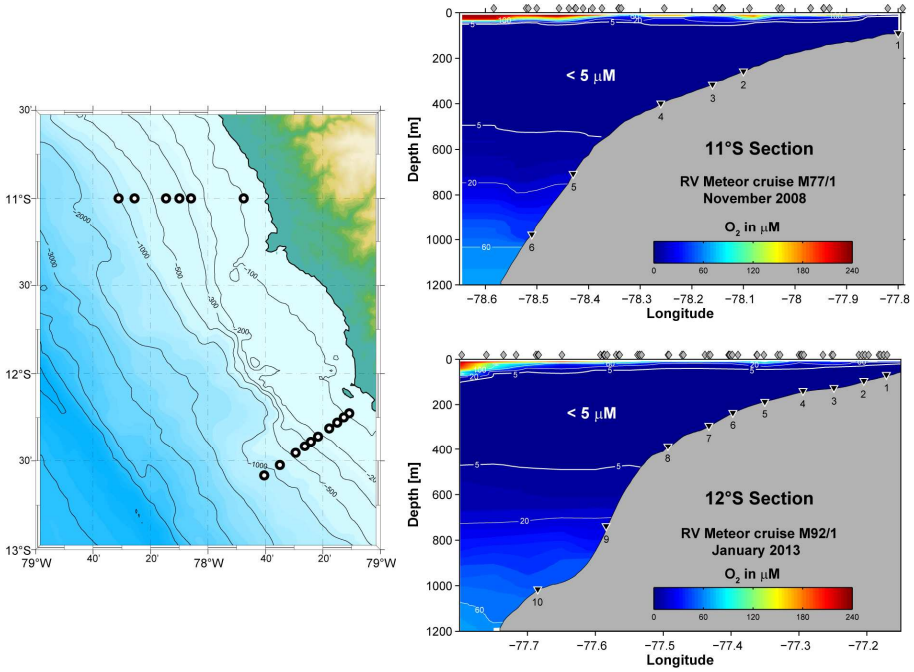

Figure 1. Slope bathymetry (m) and sampling stations on the Peruvian margin at 11° S and 12° S (left). The two panels on the right show cross-sections of dissolved oxygen concentrations (µM) measured using the CTD sensor calibrated against Winkler titrations (detection limit 5 µM). The station locations are indicated by the black triangles and the CTD stations used to make the plots are indicated by the grey diamonds.

BGD
11, 13067–13126, 2014

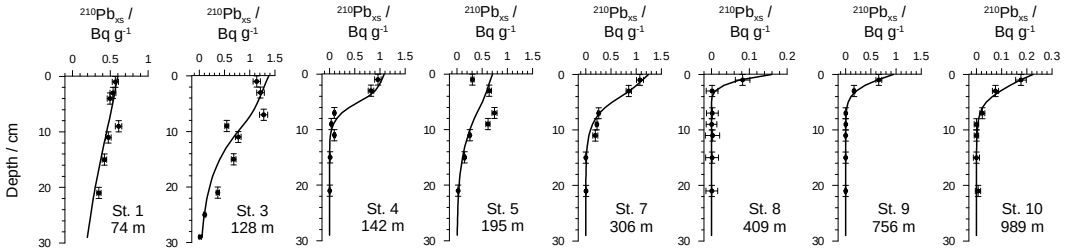

Figure 2. Measured (symbols) and modeled (curves) $^{210}Pb_{xs}$ at 12° S (see Bohlen et al. (2011) for $^{210}Pb_{xs}$ at 11° S). Vertical error bars span the depth interval from where the sample was taken, whereas horizontal error bars correspond to the analytical uncertainty. Derived upper boundary fluxes and bioturbation coefficients are listed in Table S2.

BGD
11, 13067–13126, 2014

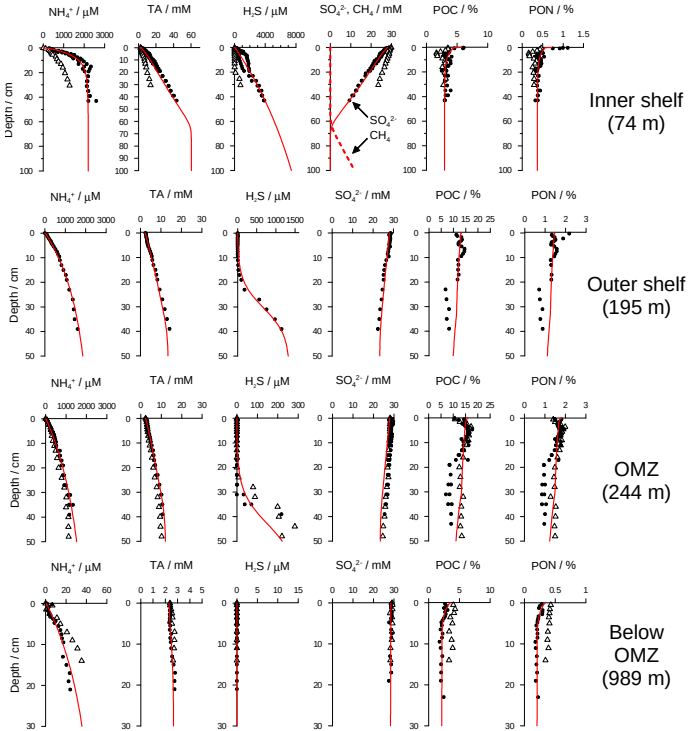

Figure 3. Dissolved and solid phase biogeochemical data for sediments core from 12° S (filled symbols) with model simulation results (red curves). Four sites are chosen to exemplify the general trends on the inner shelf (St. 1, 74 m), outer shelf (St. 5, 195 m), inside (St. 6, 244 m) and below the OMZ (St. 10, 989 m). The full set of data and model results is presented in Dale et al. (unpub. data). Also shown (open symbols) are data from three sites along 11° S (St. 1 (85 m), 3 (315 m) and 6 (978 m); Bohlen et al., 2011). For clarity, the simulation curves from 11° S have been omitted for these data and are presented in Bohlen et al. (2011). POC and PON distributions were not shown in that study and are shown for the first time here.

BGD
11, 13067–13126, 2014

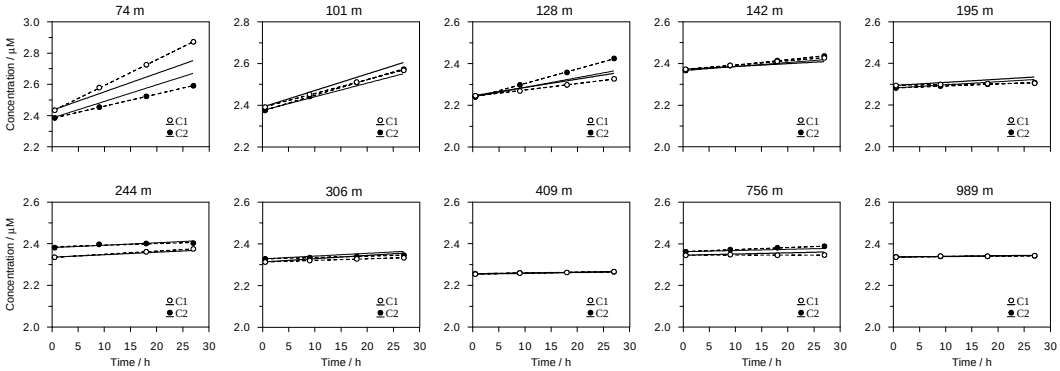

Figure 4. Dissolved inorganic carbon (DIC) concentrations inside the benthic chambers determined from measured total alkalinity (TA) and partial pressure of CO_2 (pCO_2; symbols) from 12° S. Open and filled circles refer to chamber 1 and 2, respectively. The dashed lines denote linear regression curves through the data from which the fluxes in Table 2 were calculated. The solid lines are the predicted changes in concentration using the DIC fluxes computed by the numerical model.

BGD
11, 13067–13126, 2014

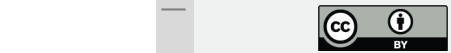

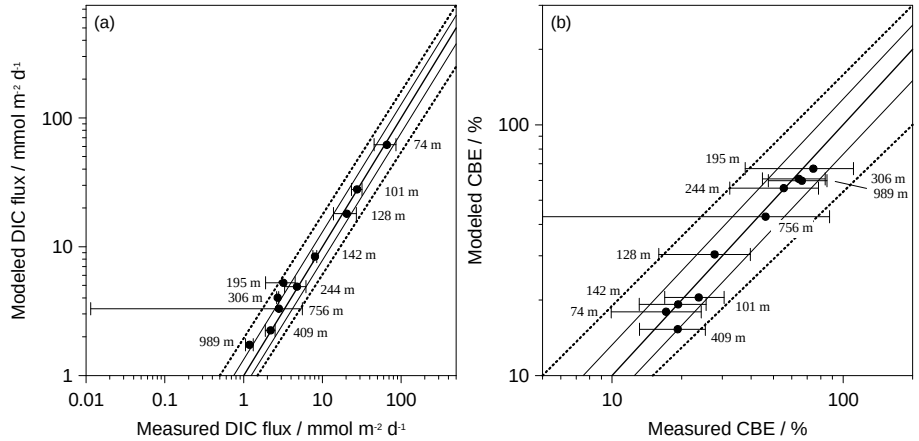

Figure 5. (a) Measured vs. modeled DIC fluxes and **(b)** measured vs. modeled carbon burial efficiencies (CBE) at 12° S. The error bars are the uncertainties in Table 2. The thick solid line is the 1 : 1 curve. The thin solid lines and dashed lines denote ±25 % and ±50 % limits on the 1 : 1 correlation, respectively.

BGD
11, 13067–13126, 2014

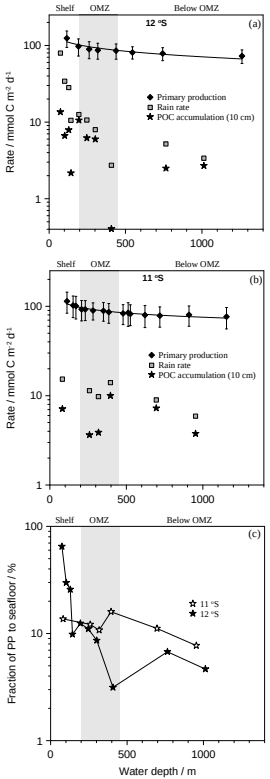

Figure 6. (a) Mean annual primary production (±s.d) for the 12° S transect calculated by the ROMS-BioEBUS model (diamonds). Rain rates to the seafloor (squares) and POC accumulation rates at 10 cm (stars) were estimated using the benthic model (Table 2). The solid line is a power law regression through the PP data. **(b)** As **(a)** for 11° S. **(c)** Fraction of PP that reaches the seafloor calculated by dividing the modeled rain rate by PP calculated from the regression curve. The grey shade highlights the OMZ stations (ca. 200 to 450 m).

BGD
11, 13067–13126, 2014

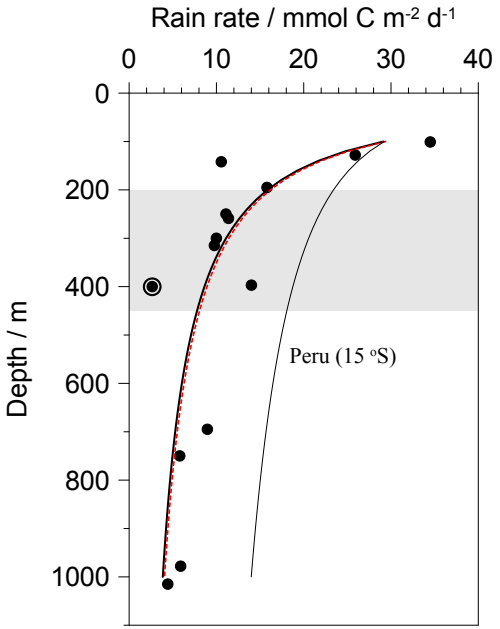

Figure 7. Organic carbon rain rate to the seafloor at 11 and 12° S (circles, modeled rates, Table 2). The thick line is the best-fit curve (Eq. 8) with an attenuation coefficient of $b = 0.88$. The datum from St. 8 (12° S) that is eroded by bottom currents is circled and not included in the regression. The dashed red line shows the flux attenuated with $b = 0.86$ derived for normal oxic waters (Martin et al., 1987). The thin line corresponds to the attenuation derived from sediment trap data offshore Peru at 15° S ($b = 0.32$, Martin et al., 1987) anchored to the rain rate at 101 m at 12° S of 28.9 mmol m^{-2} d^{-1}. The grey shade highlights the OMZ stations (ca. 200 to 450 m).

BGD
11, 13067–13126, 2014

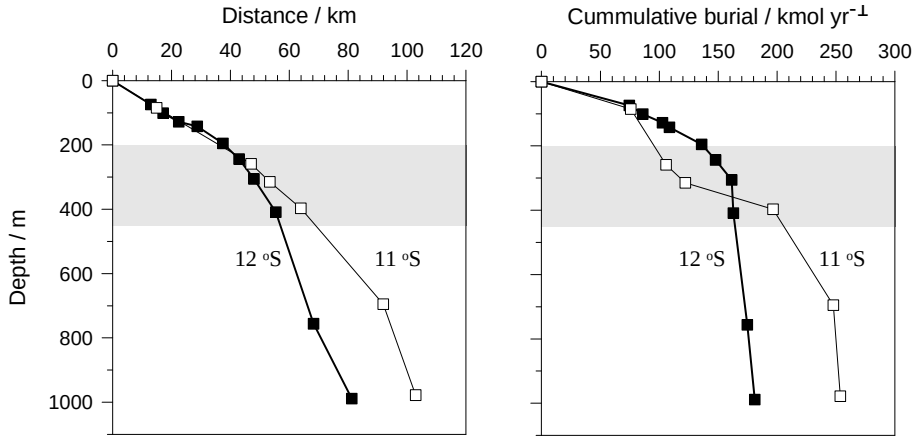

Figure 8. (a) Distance offshore vs. water depth, and **(b)** cumulative organic carbon burial at 10 cm depth, POC_{10} (measured data, Table 2) along the two transects (see text). The grey shade highlights the OMZ stations (ca. 200 to 450 m).

BGD
11, 13067–13126, 2014

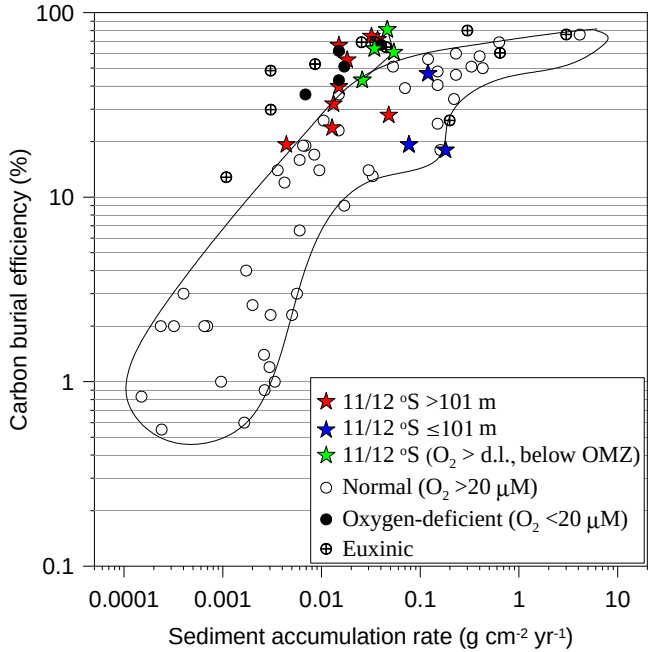

Figure 9. Carbon burial efficiency vs. bulk sediment accumulation rate in contemporary ocean sediments. Stars are data from this study for 11 and 12° S (modeled data). Blue stars indicate sites on the inner shelf, which have lower-than-expected CBE and green stars correspond to the deep oxygenated sites with higher-than-expected CBE. Most other data points are from Canfield (1993), as well as from Burdige (2007) and from studies at the continental margins of Washington State, northwest Mexico (Hartnett and Devol, 2003) and central California (Reimers et al., 1992). Open and filled circles represent sites with bottom water O_2 > 20 µM and < 20 µM, respectively; the former enclosed by the solid line. Euxinic settings are indicated separately.

BGD
11, 13067–13126, 2014